Check for updates

Received: 15 November 2023 | Revised: 16 May 2024 | Accepted: 26 May 2024

DOI: 10.1002/esp.5915

RESEARCH ARTICLE

ESPL WILEY

Unveiling the potential of karst vadose deposits in constraining Quaternary tectonic subsidence

Daniel Ballesteros[1,2] | Carlos Pérez-Mejías[3] | Diego Moreno[4] | Marcos Moreno-Sánchez[2] | Cristina Reyes-Carmona[5] | David Alfonso-Jorde[2] | José Miguel Azañón[2,6] | Guillermo Booth-Rea[2,5] | Davide Torre[7] | Paula Sofía Jerez-Longres[2] | Vicente Pérez-Peña[2] | Antonio González-Ramón[8] | Hai Cheng[2] | Jorge Pedro Galve[2] | Patricia Ruano[2,6]

[1]Departamento de Ciencias de la Tierra y Física de la Materia Condensada, Universidad de Cantabria, Santander, Spain

[2]Departamento de Geodinámica, Universidad de Granada, Granada, Spain

[3]Institute of Global Environmental Change, Xi'an Jiaotong University, Xi'an, China

[4]Agencia de Medio Ambiente y Agua, Almería, Spain

[5]Dipartimento di Scienze dell'Ambiente e della Terra, Università degli Studi di Milano-Bicocca, Milan, Italy

[6]Instituto Andaluz de Ciencias de la Tierra, CSIC-UGR, Armilla, Spain

[7]Dipartimento di Scienze della Terra, Sapienza Università di Roma, Roma, Italy

[8]Instituto Geológico y Minero de España – CSIC, Granada, Spain

Correspondence
Daniel Ballesteros, Departamento de Ciencias de la Tierra y Física de la Materia Condensada, Universidad de Cantabria, Avda. de los Castros s/n, 39005 Santander, Spain.
Email: ballesterosd@unican.es

Funding information
European Regional Development Fund, Grant/Award Number: SOE3/P4/E0868; Ministerio de Ciencia e Innovación, Grant/Award Numbers: PID2019-107138RB-I00, RYC-2017-23335; FEDER/Junta de Andalucía-Consejería de Transformación Económica, Industria, Conocimiento y Universidades/Projects; Junta de Andalucía

Abstract

In carbonate coastlines, karst studies have traditionally focused on reconstructing Quaternary coastal uplift and sea level oscillations. However, their potential for investigating coastal subsidence remains unexplored in regions with limited sedimentary records and scientific monitoring. In line with this, our study delved into the utility of karst research for deciphering the Quaternary evolution of the Granada coast in southern Spain—a shoreline marked by a conspicuous scarcity of records and information regarding recent tectonic movements. The current labelling data and the absence of evidence for uplift led to the hypothesis that the Granada coast may be susceptible to subsidence, though this conjecture remained unconfirmed. While submerged marine terraces were clearly identified, they were previously interpreted as consequences of sea-level oscillations. Our multidisciplinary approach integrated karst vadose features, biostratigraphy, and the dating of 22 speleothems to address the potential uplifting or subsiding dynamics of the Granada coast. The findings indicated that the Granada coast experienced emersion between 3.5/2.4 Ma and 650 ka ago. Notably, this uplift predated similar occurrences in neighbouring coastal regions to the W and E, which occurred within the last 200–180 ka. These disparities in timing cannot be solely attributed to sea-level fluctuations, suggesting the involvement of the tectonic activity during the Quaternary. The tectonic likely led to the emergence of the Granada coast and its karstification, followed by subsidence. Furthermore, we identified the extensional faults that caused the coastal subsidence, previously documented in studies conducted in nearby regions. However, until now, their specific impact on the Granada coast had not been comprehensively stated. In summary, our research introduces a novel application of classical karst investigations in the understanding coastal subsidence and the extensional active tectonic. By comparing vadose cave ages with established chronologies in adjacent coastal areas, this approach sheds light on the complex tectonic evolution of coastal regions.

KEYWORDS
active tectonic, coast, geochronology, karst, subsidence

This is an open access article under the terms of the Creative Commons Attribution-NonCommercial-NoDerivs License, which permits use and distribution in any medium, provided the original work is properly cited, the use is non-commercial and no modifications or adaptations are made.
© 2024 The Author(s). *Earth Surface Processes and Landforms* published by John Wiley & Sons Ltd.

1 | INTRODUCTION

Karst studies have traditionally been carried out for inferring coastal uplift worldwide (Faulkner, 2018; Smith & Moseley, 2022), with a particular focus on the Mediterranean coast (Cerrone et al., 2021; Lucia et al., 2020), the Caribbean Sea (De Waele et al., 2018; Salgado-Garrido et al., 2022) and SE of Asia (Authemayou et al., 2018; Woodhead et al., 2022). The coastal karst exhibits abundant indicators of paleo-sea-levels, encompassing features like flank margin caves (Mylroie & Mylroie, 2018), paleo-phreatic conduits (Kampolis et al., 2022), corrosion notches (Kahlert et al., 2021), phreatic speleothem overgrowths (De Waele et al., 2017) and other karst deposits (Valera-Fernández et al., 2022). Their elevation above sea level, originally formed at the water table (sea level), provides a means to quantify coastal emersion (Bini et al., 2020; Mylroie et al., 2017). The ages of these indicators are typically determined through methods such as U-decay series analysis on vadose speleothems (Weij et al., 2022), luminescence techniques on detrital sediments (Andreucci et al., 2017) and radiocarbon or biostratigraphy applied to fossil assemblages (Dumitru et al., 2021; Fedje et al., 2021).

Subsidence can affect coastal areas following a period of emersion (e.g., Corrado et al., 2022; Kanwal et al., 2022). In such cases, continental deposits (vadose salt marshes, peat bogs, deltas, lagoons, soils and Eemian deposits) and other evidence of uplift (marine terraces and tidal notches) become submerged and are frequently concealed by seawater and marine sediments (Figure 1b). This circumstance poses substantial limitations on direct observations and subsequent interpretations (Mattei et al., 2022).

While the Western Mediterranean coastline boasts numerous cliffs, marine terraces, raised beaches and emerged marine deposits (Figure 2a) (Khan et al., 2019; Rovere et al., 2023), the Granada coast (Figure 2b) stands out due to the absence of clear uplift evidence, despite its location at the base of the Betic Cordillera (3479 m elevation). This cordillera exhibits tectonic activity, but its precise understanding remains a topic of discussion. Multiple active structures have been identified in Betic Cordillera through multiple approaches, including investigations of specific tectonic features (Madarieta-Txurruka et al., 2022), seismic analysis from inland to offshore (López-Sánchez et al., 2022), magnetic susceptibility assessments (Anastasio et al., 2021), electric tomography imaging (Porras et al., 2022), gravity surveys (Tendero-Salmerón et al., 2020), Global Navigation Satellite System (GNSS) data (Galindo-Zaldívar et al., 2022), surface velocity mapping (Galve et al., 2017), relief index analysis (Medina-Cascales et al., 2021) and tufa/travertine chronology (Larrey et al., 2020). Sometimes, these methods yield controversial conclusions, necessitating the exploration of additional evidence to infer uplifting and subsiding processes.

The Quaternary tectonic history of the Granada coast remains enigmatic due to limited sedimentary records and the absence of clear uplift evidence, despite known active faults and folds in neighbouring areas. Precise levelling data suggested that Granada coast is descending at the present (Giménez et al., 2000), and Sanz de Galdeano (2006) tentatively suggested the occurrence of emerged marine terraces but lacked definitive evidence. In contrast, Martínez-Martos et al. (2016) identified buried marine terraces at depths of 26 to 110 m below sea level, linked to sea-level oscillations according to their interpretations. Thus, the Granada coast, characterized by a marble and schist shoreline, presents a potential case for active tectonics, perhaps uplift or subsidence. This context provides an ideal opportunity to apply karst records to investigate Quaternary uplift or subsidence. However, before mentioned karst indicators of paleo-sea levels are absent along the Granada coast due to their non-formation, preservation or identification. To address this gap, we conducted an investigation of vadose karst features in three study areas along the Granada coast, utilizing cave survey data, geomorphological analysis, paleontological records and speleothem dating. The applied research approach utilizes karst deposits for a novel purpose, demonstrating their potential in elucidating the long-term coastal evolution over a 10^5-year temporal scale, particularly in regions where substantial evidence of sea-level fluctuations and coastal sedimentation is lacking.

2 | STUDY AREA

The coast of Granada Province (36°44′N, 3°31′W), located in southern Spain (Figure 2b) exhibits littoral mountain ranges (up to 832 m elevation) formed during the Alpine orogeny. The coastline is dominated by cliffs up to 150 m high (Figure 3), occasionally interrupted by fluvial deltas (Fernández-Salas et al., 2007; Jabaloy-Sánchez et al., 2010, 2014), pebble-cobble bays associated with Holocene infralittoral prograding wedges (Fernández-Salas et al., 2009), and prodeltaic sedimentary formations (Bárcenas et al., 2011; Lobo et al., 2006). The shelf break is situated at approximately 110 m depth, marked by the presence of incising submarine canyons (Figure 3), located within 100–500 m from the shoreline (Cerrillo-Escoriza et al., 2023; Ortega-Sánchez et al., 2014). The coastal landscape has been subject to modifications resulting from landslides and human activities (Barra et al., 2022; Mateos et al., 2017; Notti et al., 2015), exacerbating local coastline retreat (Bergillos & Ortega-Sánchez, 2017), within the context of ongoing local sea-level rise (Serrano et al., 2020).

The climate of the Granada coast is Mediterranean, classified as Csa according to the Köppen–Geiger climate classification, characterized by temperate winters and warm, arid summers (Cunha et al., 2011). The average annual temperature is 18°C, with an annual precipitation of approximately 420 mm and very high evapotranspiration rates. The climate was predominantly dry over the past 200 ka, as indicated by nearby Quaternary records (Álvarez-Lao et al., 2009; Jordá Pardo et al., 2011), with a positive precipitation/evapotranspiration balance during glacial periods (Camuera et al., 2018).

The Granada coast is situated within the internal zone of the Betics-Rif orogen, an arc-shaped mountain belt surrounding the Gibraltar strait, formed by the convergence between the European and African tectonic plates from the late Cretaceous to the present day (see Gómez de la Peña et al., 2021, and references therein). In detail, the geological composition of the Granada coast consists of Palaeozoic-Triassic phyllite, quartzite and schist-, and Triassic marble (Figure 3) (see Marín-Lechado et al., 2009). The geological structure comprises recumbent folds, with minor folds observed in their limbs, influenced by major and local faults, as well as a high density of joints and tectonic foliations (Azañón & Crespo-Blanc, 2000; Simancas, 2018). The Triassic marble is traditionally regarded as a karst aquifer with significant fissueation and a low degree of internal karstification (Andreo et al., 2018; Montiel et al., 2018). This

10969837, 2024, 11, Downloaded from https://onlinelibrary.wiley.com/doi/10.1002/esp.5915 by CochraneItalia, Wiley Online Library on [18/10/2024]. See the Terms and Conditions (https://onlinelibrary.wiley.com/terms-and-conditions) on Wiley Online Library for rules of use; OA articles are governed by the applicable Creative Commons License

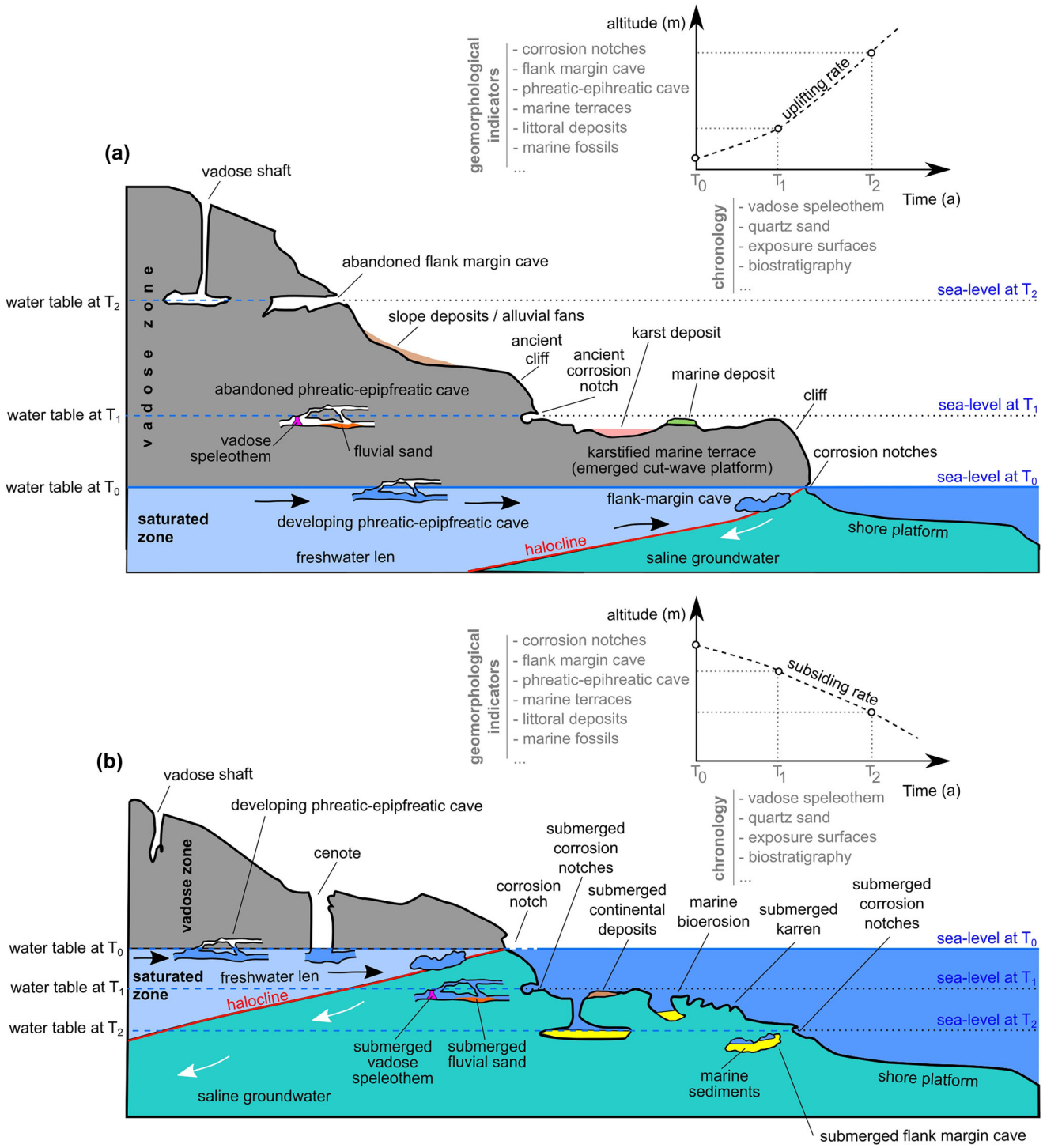

FIGURE 1 Karst cave features commonly employed as geomorphological indicators of coastal uplift (a) and sea-level rising (b) provide valuable insights into the Quaternary evolution of coastlines composed of calcareous rocks (after Bini et al., 2020; Mylroie & Mylroie, 2018; Mylroie et al., 2017; Van Hengstum et al., 2015). Flak margin caves are mixing dissolution chambers formed in the contact between fresh and saline groundwaters; phreatic-epiphreatic caves derived from fresh phreatic groundwater flow. Calculation of potential coastal uplifting or sea-level rising rates would be stated by the combination of geomorphological indicators and chronological data. [Color figure can be viewed at wileyonlinelibrary.com]

aquifer is bounded by schist, quartzite and phyllite of low permeability and extends inland (Figure 3), where the primary recharge occurs through rain infiltration via karst surfaces and depressions (Andreo et al., 2018; González-Ramón et al., 2017; López-Chicano et al., 2002; Martos-Rosillo et al., 2015). Groundwater exchange occurs between karst and detrital coastal aquifers, constrained by saltwater intrusions (Calvache et al., 2020) and tidal influences (Blanco-Coronas et al., 2021, 2022). The primary discharge of the karst aquifer occurs through springs, with some, such as those at Cantarriján beach and Cerro Gordo cape outlets (Figure 3), being submarine, as evidenced by the occurrence of low-salinity seawater and anomalies in ^{222}Rn and 224Ra offshore (Montiel et al., 2018). Speleological groups (*Grupo de Actividades Espeleológicas de Motril* and others) have reported the existence of karst caves within three marble coastal areas, which form the focal points of this study (Figure 3): (1) Cerro Gordo cape, (2) Punta de la Mona cape and (3) Calahonda karst. These capes feature promontories at altitudes

10969837, 2024, 11, Downloaded from https://onlinelibrary.wiley.com/doi/10.1002/esp.5915 by CochraneItalia, Wiley Online Library on [18/10/2024]. See the Terms and Conditions (https://onlinelibrary.wiley.com/terms-and-conditions) on Wiley Online Library for rules of use; OA articles are governed by the applicable Creative Commons License

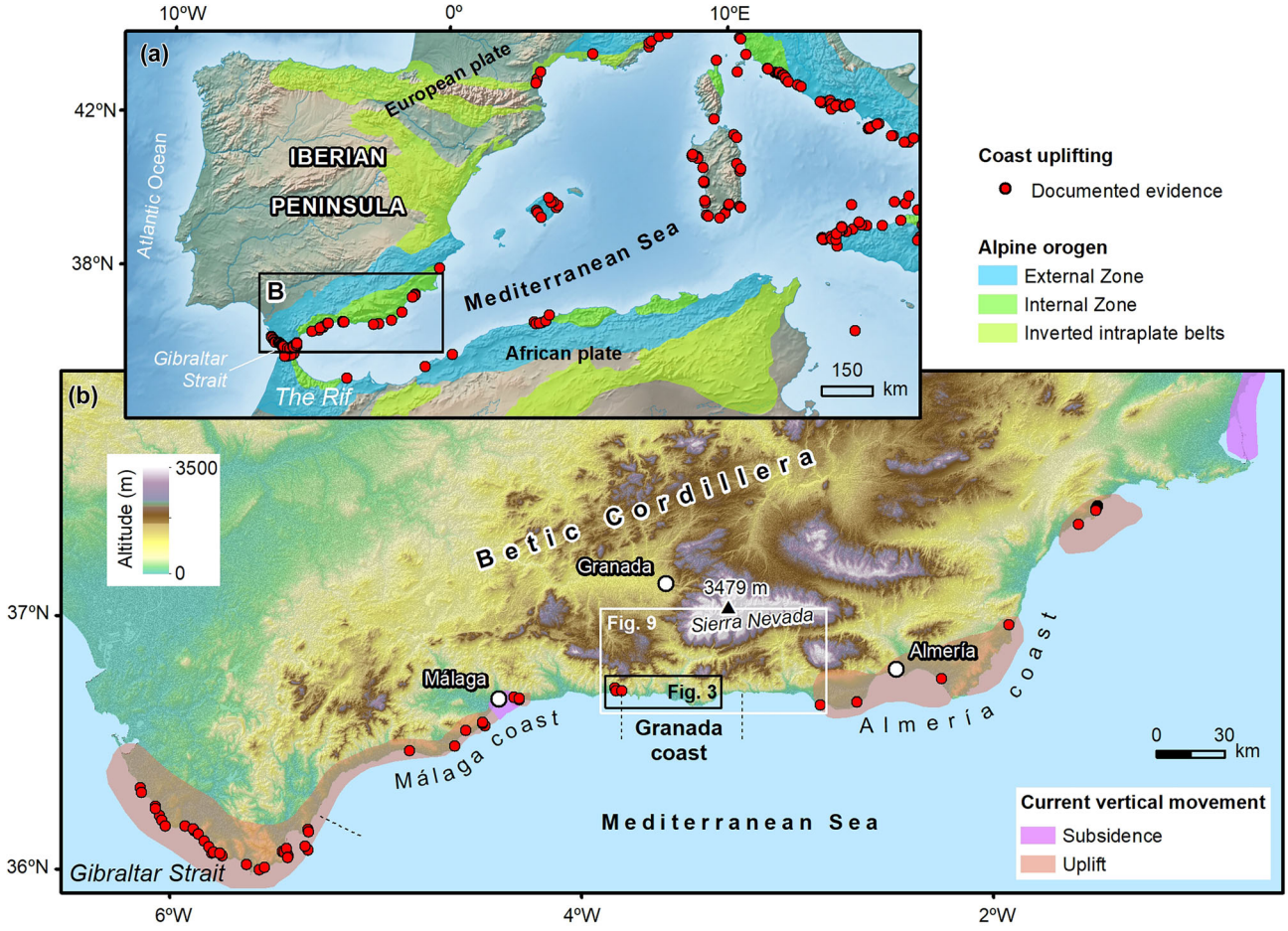

FIGURE 2 (a) Sea-level indicators related to the Betic-Rif orogen in the Western Mediterranean Sea according to the Atlas of Last Interglacial Shorelines-WALIS (Khan et al., 2019; Rovere et al., 2023). Zones of the Betic-Rif orogen are after Moragues et al. (2021). (b) Southern Iberian Peninsula showing uplift evidence detailed in many geomorphological studies (Bardají et al., 2015, 2022; Goy et al., 2003; Goy & Zazo, 1986, 1989; Hillaire-Marcel et al., 1986; Lario et al., 1993; Zazo et al., 1984, 1994, 1999, 2003, 2008, 2013; Zazo & Goy, 1989, and references therein) and reported coastal areas affected by uplifting or subsiding (after Galve et al., 2020). [Color figure can be viewed at wileyonlinelibrary.com]

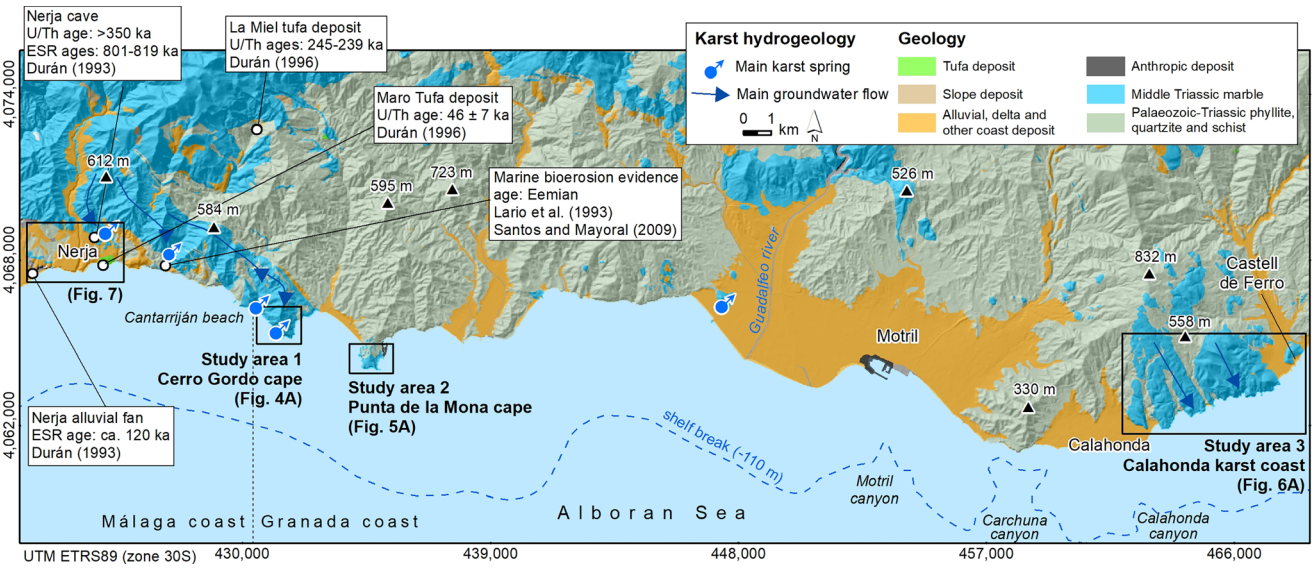

FIGURE 3 Geology and karst of Granada coast showing the three study areas: Cerro Gordo and Punta de la Mona capes, and Calahonda karst area. Reported evidence of coastal uplifting are indicated. The geology is after Marín-Lechado et al. (2009); karst springs and groundwater flow are from Calvache and Pulido-Bosch (1993, 1997), Andreo et al. (2018) and Montiel et al. (2018); the shelf break is after Bárcenas et al. (2011). The location of the figure is shown in Figure 2b. [Color figure can be viewed at wileyonlinelibrary.com]

10969837, 2024, 11, Downloaded from https://onlinelibrary.wiley.com/doi/10.1002/esp.5915 by CochraneItalia, Wiley Online Library on [18/10/2024]. See the Terms and Conditions (https://onlinelibrary.wiley.com/terms-and-conditions) on Wiley Online Library for rules of use; OA articles are governed by the applicable Creative Commons License

of 232 and 126 m, located in the westernmost section of the Granada coast. To the east, Calahonda karst encompasses minor capes, cliffs, coves and steep slopes between the Calahonda and Castell de Ferro villages.

3 | METHODOLOGY

The conventional application of karst studies for deducing the evolution of a calcareous coastline primarily relies on phreatic cave features and submerged/phreatic speleothems formed at the water table (sea level) in the past (see Mylroie & Mylroie, 2018; Van Hengstum et al., 2015). However, in the Granada coast, such features have not been identified, at least not within the explored emerged karst. This absence can be attributed to the extensive fracturing and limited karstification of the marble aquifer (Andreo et al., 2018; Montiel et al., 2018) due to the low annual precipitations along the last 200 ka. To bridge this knowledge gap, we have turned to vadose deposits following Van Hengstum et al. (2015) and Lucia et al. (2020). The deposits of continental origin (vadose speleothems and land fossils) help us gain insights into areas that have already emerged at different times. This approach enables us to make tentative estimates of the maximum sea level (Van Hengstum et al., 2015) and the minimum extent of the vadose zone during different periods using vadose speleothems ages (Figure 4). The methodological approach relies on considering only the oldest speleothems at each elevation as reference points. It is crucial that the ages of all considered speleothems remain internally consistent, establishing a chronological sequence that increases in age with altitude. These historical boundaries are depicted by isochrones, although their positions are approximations due to inherent method limitations.

3.1 | Cave geomorphology survey

Cave geomorphology analysis was conducted to characterize the karst cavities along the Granada coast, utilizing speleological survey data and mapping of vadose features performed during fieldwork. The karst caves explored and surveyed by the Grupo de Actividades Espeleológicas de Motril (Spain) were integrated into ArcGIS to comprehensively analyse their geometry and morphology. The workflow, as detailed in Ballesteros et al. (2015), involved the following steps: compilation of UTM coordinates for cave entrances; collection of original survey cave data generously provided by speleological groups; restoration of virtual cave survey lines from historical cave maps; and generation of a shapefile containing cave survey 3D lines within Compass software. This included polar coordinates such as real length, direction and dip, as well as vertical and horizontal diameters of cave passages and projection of cave entrances and survey 3D lines within ArcGIS for comprehensive analysis and visualization.

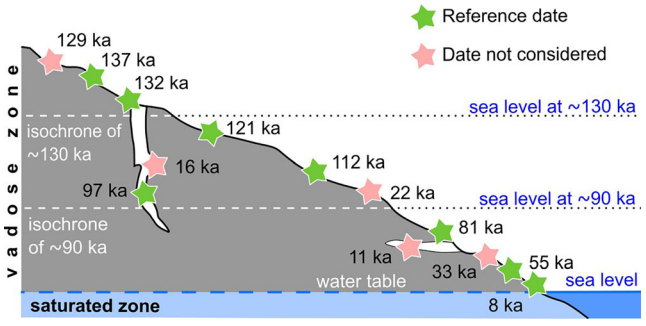

FIGURE 4 Conceptual model illustrating the use of vadose karst deposits to estimate the vertical extent of the vadose zone at different time intervals. Each time is associated with tentative isochrones determined by the chronology of the oldest vadose speleothems for each altitude. Younger speleothems at each altitude are not considered. Age values are provided solely for illustrative purposes. [Color figure can be viewed at wileyonlinelibrary.com]

3.2 | Vadose speleothem ages

Twenty-two strategically selected karst deposits were sampled and dated using the U/Th method to establish their chronology. The objective was to target vadose speleothems formed directly on the bed-rock to approximate the minimum age of the karst features. However, the study area caves were rich in speleothems and breakdown deposits, making it challenging to meet our sampling requirements. To address this, we opted to sample speleothems from the exokarst, where the contact between flowstone and bed-rock is exposed. In total, we collected 15 flowstones from the exokarst surface and four speleothems from the endokarst along the Granada coast. In addition, three samples have been collected from the Málaga coast to support the further interpretations. Among these, two flowstone samples preserved in the exokarst in Nerja, while the third was obtained from a tufa deposit near Maro, previously investigated by Durán (1996). Optical microscopy analysis revealed that all speleothem samples exhibited columnar textures without any diagenetic features, such as micritized crystals, lateral overgrowths or corrosion evidence. This suggests that the geochemical system remained closed after precipitation. The procedures for sampling, sample preparation, laboratory processes and calculations employed in the speleothem dating follow Cheng et al. (2000) and are detailed in Section 1 of the supporting information. Speleothem ages were reported in years before present (1950), along with associated two sigma (2σ) uncertainties.

4 | RESULTS

4.1 | Karst caves and speleothems

In the Cerro Gordo cape (study area 1), 11 caves with a total length of 330 m are documented (Figure 5a), as well as unroofed and filled karst cavities preserved at the surface. Here, the sample GOR-11 was collected at 178 m elevation from a speleothem formed within a relict cave with fracture shape (Figure 5b). Las Palomas cave (Figure 5c), a marine cavity measuring 110 m in length with a 35-m vertical range, was formed by wave action along a local phyllite bed inclined at 40° to the SW. Within the cave, a ramp of marble boulders is covered by small flowstone and stalagmites at the upper part (Figure 5d). Samples GOR-12 and GOR-13 were collected from flowstone and stalagmite formations directly atop a fallen boulder. Espinosa cave, a fracture-shaped shaft spanning 128 m in length and with a vertical range of 128 m,

10969837, 2024, 11, Downloaded from https://onlinelibrary.wiley.com/doi/10.1002/esp.5915 by CochraneItalia, Wiley Online Library on [18/10/2024]. See the Terms and Conditions (https://onlinelibrary.wiley.com/terms-and-conditions) on Wiley Online Library for rules of use; OA articles are governed by the applicable Creative Commons License

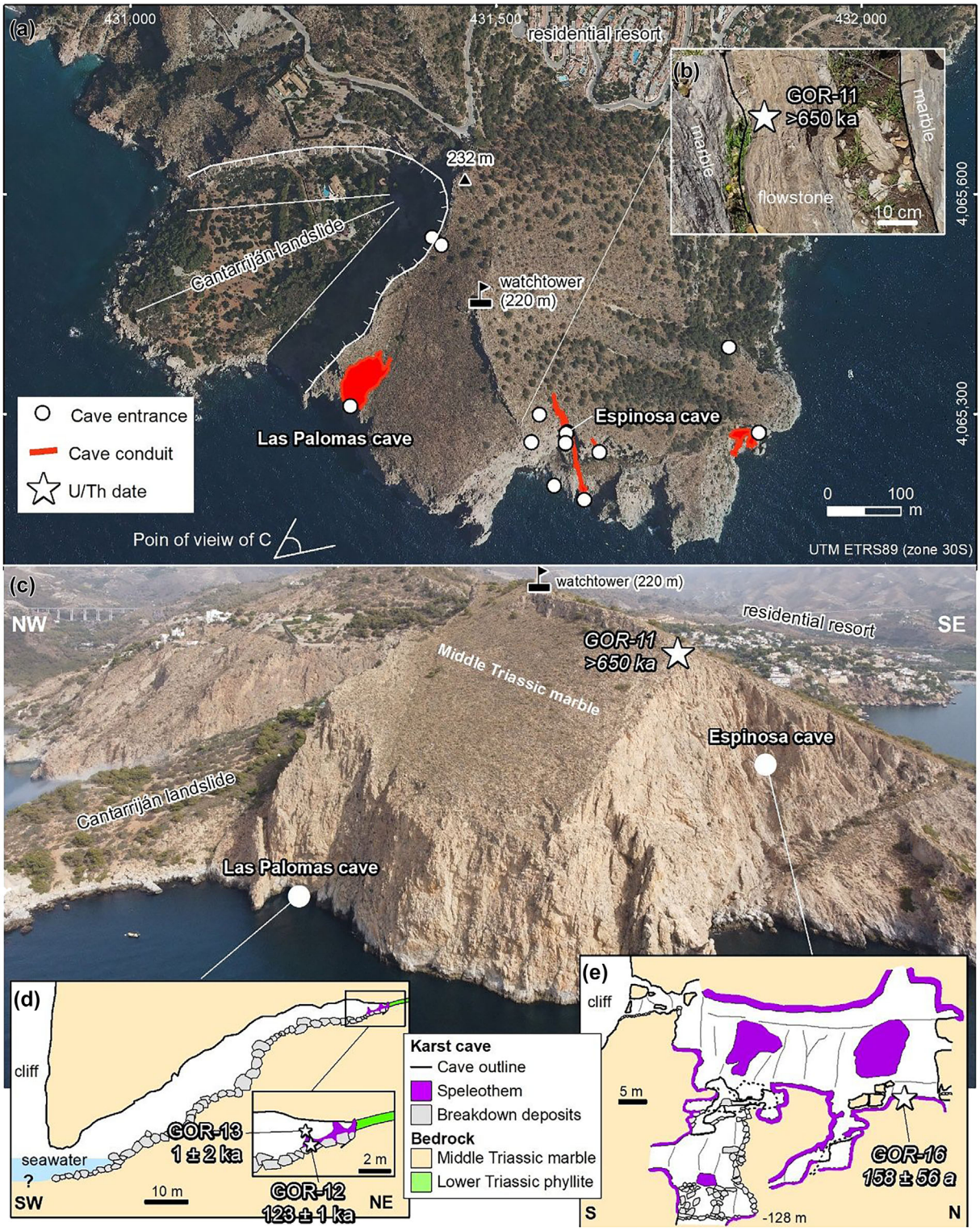

FIGURE 5 (a) Karst area of Cerro Gordo cape (study area 1 of Figure 3) showing the main karst caves and speleothem dates. (b) View of the Cerro Gordo cape from the S. (c) Longitudinal section of Las Palomas cave; showing the dated stalagmite (the cave survey is courtesy of Grupo de Actividades Espeleológicas de Motril). (d) Extended longitudinal profile of the Espinosa shaft (surveyed by Comité Départamental de Spéléologie du val d'Oise), where the dated flowstone is depicted. [Color figure can be viewed at wileyonlinelibrary.com]

developed along a N–S trending fracture. This cave boasts abundant breakdown deposits and numerous speleothems, including dripstone and flowstone formations on the cave walls and ceiling. Sample GOR-16 was acquired from a flowstone within the cavity (Figure 5e).

The Punta de la Mona cape (study area 2) only shows relict caves with fracture form and filled by speleothems (Figure 6a). A sample of flowstone PLM-02 was collected from a fracture located at an altitude of 58 m while flowstone PLM-01 is associated with a 40 m-long fracture located at the southeastern most cape (Figure 6b). The fracture displays flowstones and stalactites precipitated on the fracture walls (Figure 6c,d), as well as a cemented detrital infill with gastropods (see Section 4.2) deposited on speleothems.

Speleological expeditions have recently documented 78 karst caves within the Calahonda karst region (study area 3), extending over

10969837, 2024, 11, Downloaded from https://onlinelibrary.wiley.com/doi/10.1002/esp.5915 by CochraneItalia, Wiley Online Library on [18/10/2024]. See the Terms and Conditions (https://onlinelibrary.wiley.com/terms-and-conditions) on Wiley Online Library for rules of use; OA articles are governed by the applicable Creative Commons License

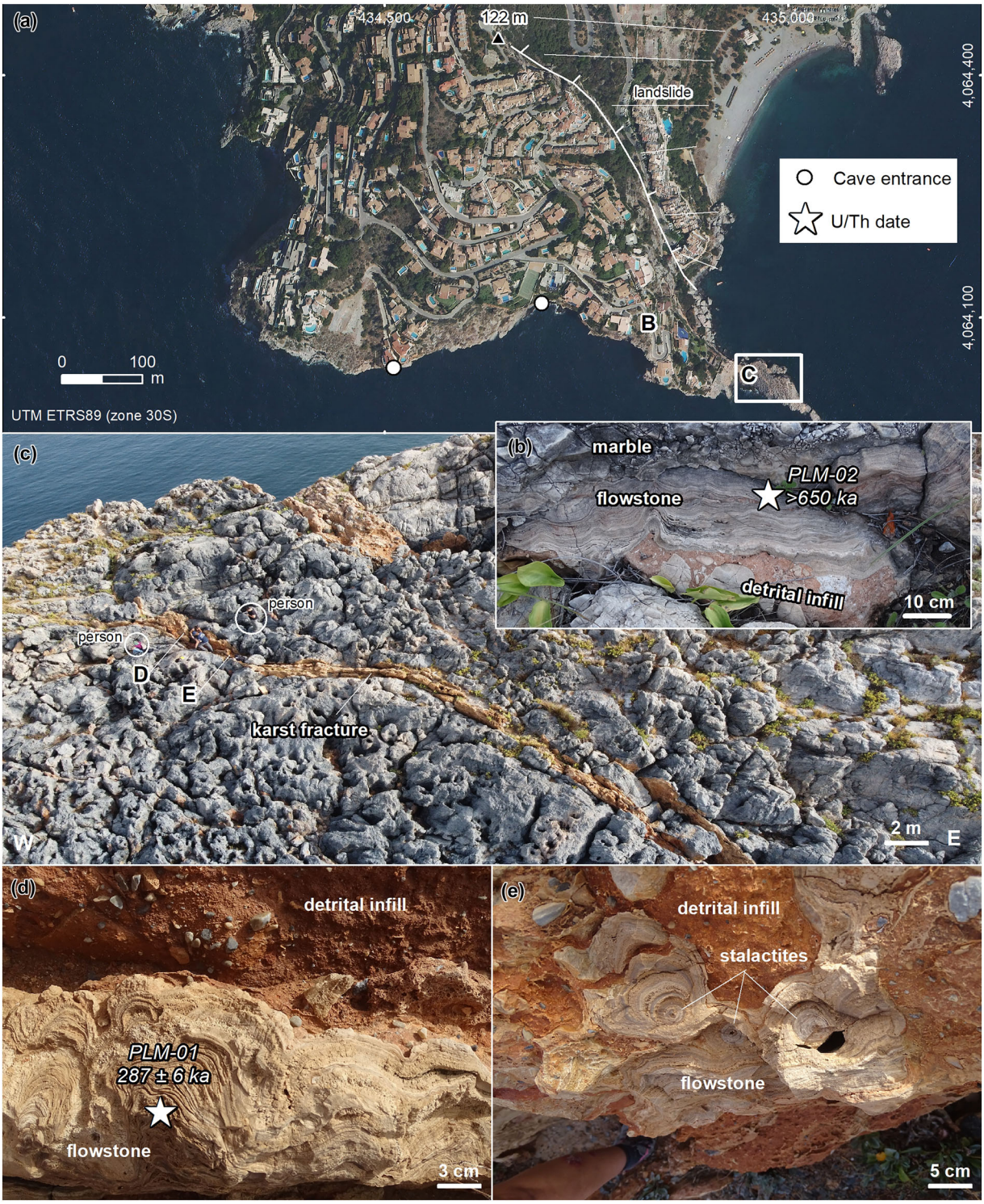

FIGURE 6 (a) Karst area of the Punta de la Mona cape (study area 2 of Figure 3) showing the main karst caves (without significant speleothems) and the position of the studied fracture. (b) Flowstone PL-02 precipitated within a fracture. (c) Fracture examined in the southeastern most cape, where the speleothem PLM-01 was collected. (d) Top view of flowstone PLM-01 precipitated on fracture walls. (e) Top view of other speleothems covered by detrital cave deposits. [Color figure can be viewed at wileyonlinelibrary.com]

a cumulative length of approximately 3.8 km. These caves are distributed across an elevation range from sea level to approximately 600 m (Figure 7). They exhibit the distinctive form of vadose fracture-shaped canyons and shafts (see Figure S1A–C for visual reference), with depths reaching up to 78 m. Within these cave systems, one can observe straight passages characterized by rectangular transversal sections, with dimensions typically spanning between 0.5 to 2 m in width and a height of less than 20 m. Cave passages have partial fillings composed of breakdown deposits, speleothems (including substantial flowstones and well-formed dripstones), and detrital sediments (Figure S1C–F).

The cave formation primarily arose from the expansion of existing fractures, bedding planes and tectonic foliations. The presence of speleothems is a prevalent feature within the Calahonda karst, with these formations cover frequently the entirety of cave walls and floors. This dense speleothem coverage often complicates the

10969837, 2024, 11, Downloaded from https://onlinelibrary.wiley.com/doi/10.1002/esp.5915 by CochraneItalia, Wiley Online Library on [18/10/2024]. See the Terms and Conditions (https://onlinelibrary.wiley.com/terms-and-conditions) on Wiley Online Library for rules of use; OA articles are governed by the applicable Creative Commons License

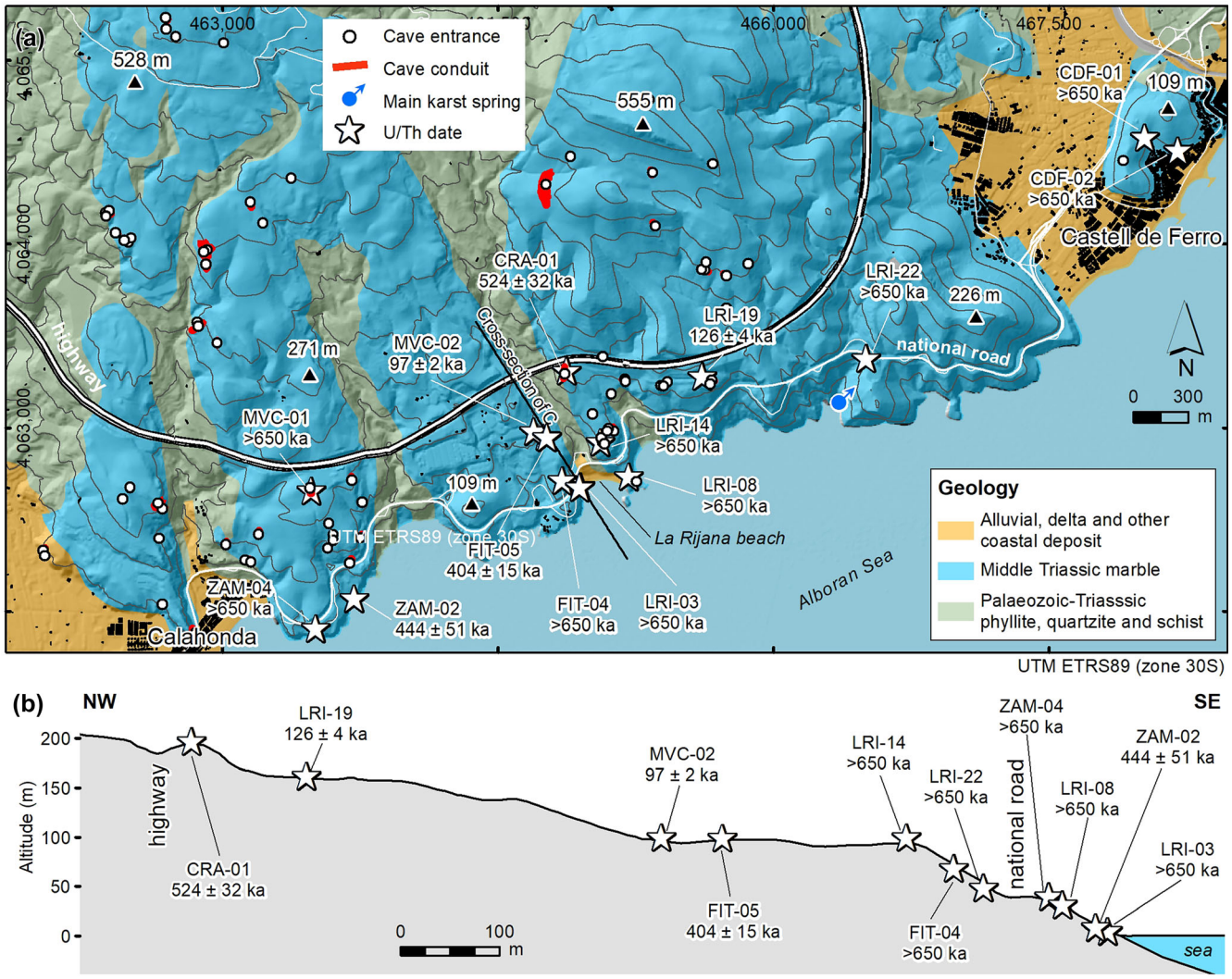

FIGURE 7 (a) Calahonda karst area (study area 3 of Figure 3) showing main karst caves. The geology is after Marín-Lechado et al. (2009) and cave surveys are from *Grupo de Actividades Espeleológicas de Motril*. (b) U/Th dates projected on a NW–SE cross-section whose location is shown in (a). [Color figure can be viewed at wileyonlinelibrary.com]

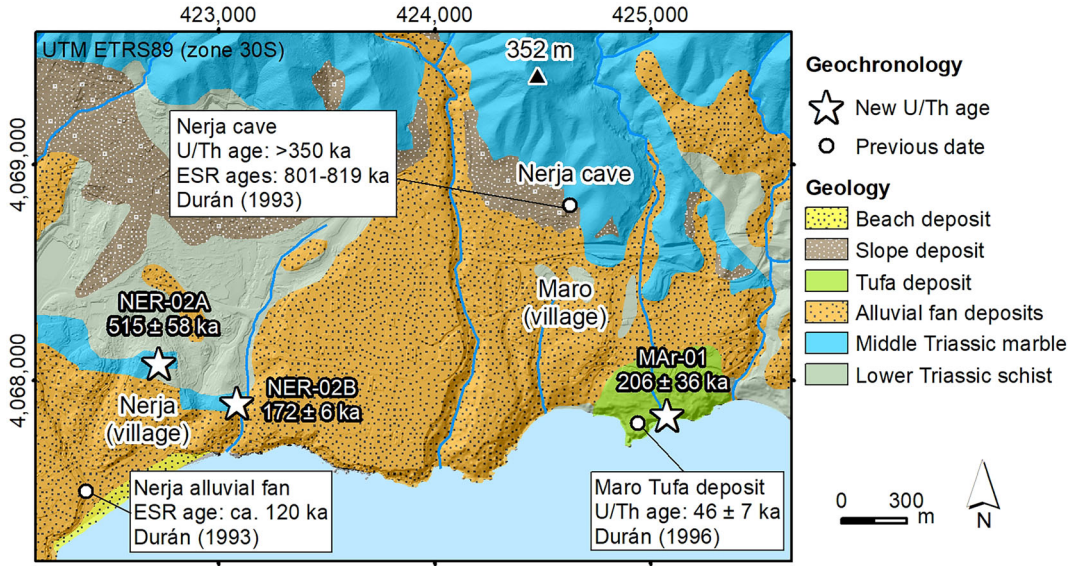

FIGURE 8 Nerja area (Málaga coast) where three samples have been collected to support the further discussion. The geomorphology and geology are after Guerra-Merchán et al. (2004) and Marín-Lechado et al. (2009). The location of Figure 8 is shown in Figure 3. [Color figure can be viewed at wileyonlinelibrary.com]

10969837, 2024, 11, Downloaded from https://onlinelibrary.wiley.com/doi/10.1002/esp.5915 by CochraneItalia, Wiley Online Library on [18/10/2024]. See the Terms and Conditions (https://onlinelibrary.wiley.com/terms-and-conditions) on Wiley Online Library for rules of use; OA articles are governed by the applicable Creative Commons License

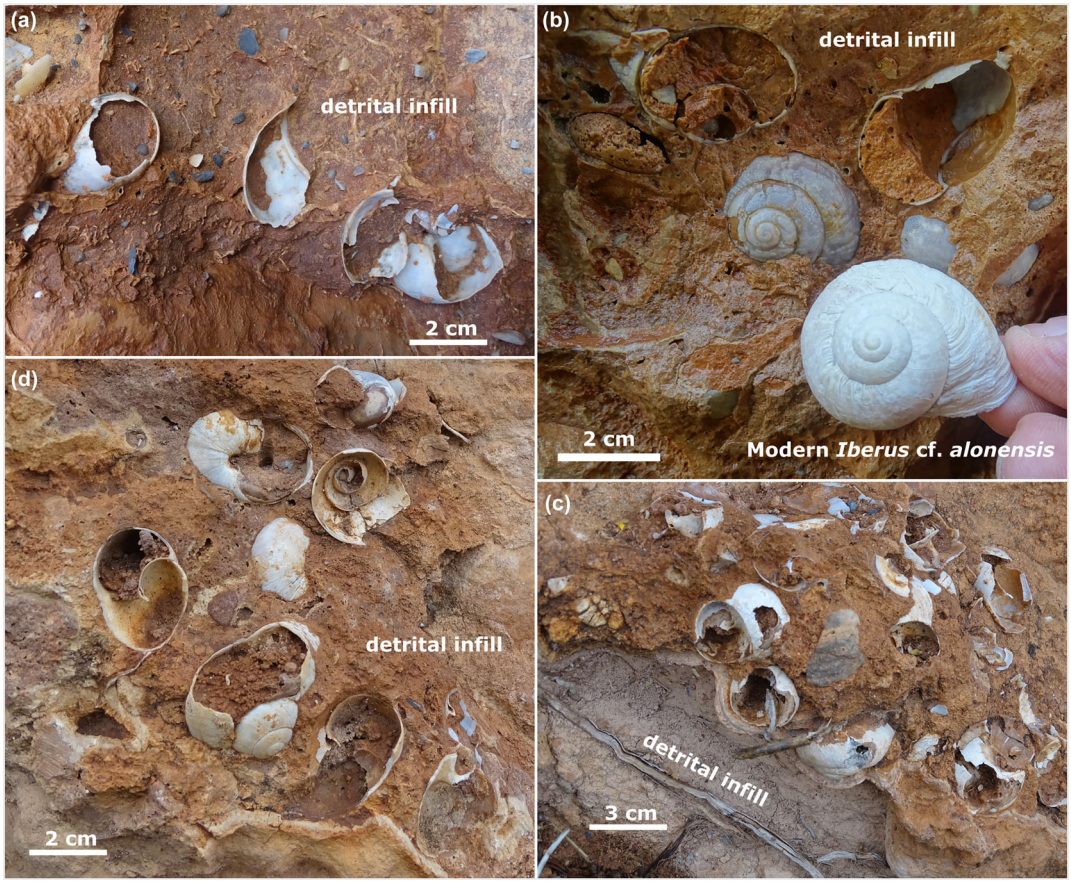

FIGURE 9 *Iberus* cf. *alonensis* preserved within karst deposits from the Granada coast: (a, b) fossil remains in Punta de la Mona cape (study area 2) and (c, d) fossil shells discovered in the Calahonda karst (study area 3). Panel (b) shows the comparison between a fossil shell and a modern *Iberus* cf. *alonensis* from the study area (Frigiliana, Province of Málaga), belonging to the personal collection of D. Moreno. [Color figure can be viewed at wileyonlinelibrary.com]

collection of direct samples from the flowstone bottom. However, erosion processes regularly unveil solidified cave infill at the surface, clearly exposing the juncture between speleothems and underlying bed-rock. In this specific geological context, vadose flowstones have managed to endure and persist within the karst caves and infill deposits. Fourteen flowstone samples were meticulously collected, spanning from the tidal zone to an elevation of 220 m (Figure 7b).

Furthermore, to enhance our discussion, we carried out three new U/Th dating analyses along the Málaga coast (Figure 8). Our comprehensive research in this coastal region primarily concentrated on the geomorphology (Guerra-Merchán et al., 2004; Lario et al., 1993, and references therein), with a particular focus on the Nerja cave, situated at an altitude of 150 m (Durán, 1996). Within the vicinity of Nerja village, we extracted two speleothems within excavations at elevations of 75 and 30 m, namely, NER-02A and NER-02B. Additionally, we determined a new age for the Maro tufa deposit for confirming the previous chronology carried out by Durán (1996).

4.2 | Paleontological evidence

Gastropod shells have been discovered within karst deposits from both Punta de la Mona cape and Calahonda karst (Figure 9). The gastropods are pulmonate land snails belonging to the genus *Iberus*, which is endemic to the Iberian Peninsula. This discovery confirms that karst infill is of continental origin. The shells correspond probably to *Iberus alonensis* according to their size (3–4 cm diameter), globular shape without keel (Figure 9b) and geographic and temporal distribution (Elejalde et al., 2005). It is worth noting that *Iberus* is a polyphyletic genus consisting of highly variable and polymorphic species, as well as many cases of hybridization. Thus, its taxonomy is currently being debated based on ongoing molecular polygenic analysis (Elejalde et al., 2008; Neiber et al., 2021). According to Neiber et al. (2021), the divergence time between *Iberus* cf *alonensis* and other related taxa would occur between 3.5 and 2.4 million years ago, providing a maximum reference age for the gastropod fossils found along the Granada coast.

4.3 | Speleothem ages

The speleothem samples analysed by U/Th dating (Table 1) exhibit the requisite content of ^{238}U for the dating method, ranging usually between 100 and 300 ppb. Notably, GOR samples stand out with values reaching up to 2 and 7 ppm, which further substantiates the robustness of the ages. The possibility of contamination by detrital ^{230}Th is not relevant for most samples as is suggested by high $^{230}Th/^{232}Th$ ratios (>10). Overall, the obtained chronological data are robust and reliable. Among the samples, 10 are in secular equilibrium ($^{230}Th/^{238}U \approx 1$) with low $\delta\,^{234}U$ measured, and thereby, its precipitation took place prior to 650 ka. The remaining 12 speleothems cover a wide time range, from recent times to going back near the limit of

10969837, 2024, 11, Downloaded from https://onlinelibrary.wiley.com/doi/10.1002/esp.5915 by CochraneItalia, Wiley Online Library on [18/10/2024]. See the Terms and Conditions (https://onlinelibrary.wiley.com/terms-and-conditions) on Wiley Online Library for rules of use; OA articles are governed by the applicable Creative Commons License

TABLE 1 U-Th ages of speleothem collected in Granada coast and surroundings of Nerja (Málaga coast).

Sample number	Altitude (m)	^{238}U ppb	^{232}Th ppt	$^{230}Th/^{232}Th$ Atomic $\times 10^{-6}$	$\delta\ ^{234}U$[a] Measured	$^{230}Th/^{238}U$ Activity	^{230}Th age Uncorrected a	$\delta\ ^{234}U_{Initial}$[b] Corrected	^{230}Th Age[c] Corrected a BP
GOR-11	188	240.0 ± 0.9	2676 ± 54	1488 ± 30	7.0 ± 3.7	1.0057 ± 0.0040			>650 000
GOR-12	31	7323.3 ± 31.5	601 ± 12	136 077 ± 2838	0.5 ± 2.0	0.6777 ± 0.0032	123 346 ± 1193	1 ± 3	123 344 ± 1192
GOR-13	31	2206.3 ± 9.0	199 715 ± 4062	7 ± 0	15.5 ± 7.3	0.0366 ± 0.0008	4005 ± 92	16 ± 7	1309 ± 1859
GOR-16	121	7875.4 ± 62.2	21 044 ± 455	17 ± 1	4.9 ± 14.3	0.0028 ± 0.0001	306 ± 11	5 ± 14	158 ± 56
PLM-01	4	150.9 ± 0.2	3731 ± 78	661 ± 14	51.2 ± 2.3	0.9905 ± 0.0032	287 540 ± 5883	115 ± 6	286 820 ± 5868
PLM-02	50	371.4 ± 0.8	11 871 ± 239	517 ± 10	1.3 ± 1.8	1.0028 ± 0.0025			>650 000
MVC-02	112	101.9 ± 0.3	9669 ± 195	112 ± 2	70.4 ± 4.3	0.6470 ± 0.0032	99 723 ± 1080	93 ± 6	97 096 ± 2088
FIT-04	71	46.1 ± 0.1	2631 ± 53	290 ± 6	4.9 ± 1.8	1.0043 ± 0.0021			>650 000
FIT-05	99	156.0 ± 0.3	8945 ± 180	282 ± 6	3.3 ± 1.9	0.9803 ± 0.0024	406 035 ± 15 585	10 ± 6	404 296 ± 15 385
ZAM-02	14	279.1 ± 1.2	58 945 ± 1203	81 ± 2	35.6 ± 4.0	1.0323 ± 0.0066	449 529 ± 53 292	125 ± 23	443 852 ± 50 631
ZAM-04	51	123.0 ± 0.1	1004 ± 20	2050 ± 41	10.7 ± 1.5	1.0144 ± 0.0016			>650 000
CRA-01	183	188.9 ± 0.2	4007 ± 80	777 ± 16	5.9 ± 1.3	1.0001 ± 0.0016	524 934 ± 32 137	26 ± 6	524 247 ± 31 953
LRI-03	1	198.8 ± 0.3	33 619 ± 674	99 ± 2	7.6 ± 1.5	1.0135 ± 0.0020			>650 000
LRI-08	39	225.8 ± 1.2	312 293 ± 6252	13 ± 0	75.2 ± 5.3	1.1203 ± 0.0071			>650 000
LRI-14	114	165.1 ± 0.1	11 280 ± 226	246 ± 5	4.4 ± 1.0	1.0188 ± 0.0020			>650 000
LRI-19	158	158.9 ± 0.1	27 589 ± 556	67 ± 1	4.2 ± 1.2	0.7027 ± 0.0028	131 008 ± 1075	6 ± 2	125 793 ± 3782
LRI-22	46	145.0 ± 0.1	37 015 ± 741	66 ± 1	13.8 ± 1.2	1.0249 ± 0.0035			>650 000
CDF-01	71	125.1 ± 0.5	3444 ± 70	600 ± 12	1.3 ± 3.8	1.0022 ± 0.0045			>650 000
CDF-02	28	269.4 ± 0.9	107 521 ± 2181	42 ± 1	12.7 ± 3.9	1.0247 ± 0.0068			>650 000
NER-02A	61	353.9 ± 0.5	163 346 ± 3274	36 ± 1	18.5 ± 1.5	1.0179 ± 0.0043	527 969 ± 65 814	79 15	514 690 ± 58 293
NER-02B	36	215.2 ± 0.6	11 975 ± 242	257 ± 6	72.4 ± 3.3	0.8661 ± 0.0128	173 481 ± 6308	118 6	171 951 ± 6310
MAR-01	26	591.7 ± 2.5	859 749 ± 17 557	11 ± 0	69.3 ± 4.6	0.9840 ± 0.0090	255 268 ± 10 408	125 15	209 509 ± 35 905

Note: Error is expressed as two times the standard deviation (2σ). U decay constants: $l_{238} = 1.55125 \cdot 10^{-10}$ (Jaffey et al., 1971) and $l_{234} = 2.82206 \cdot 10^{-6}$ (Cheng et al., 2013); Th decay constant: $l_{230} = 9.1705 \cdot 10^{-6}$ (Cheng et al., 2013). Corrected ^{230}Th ages assume the initial $^{230}Th/^{232}Th$ atomic ratio of 4.4 ± 2.2 $\cdot 10^{-6}$. Those are the values for a material at secular equilibrium, with the bulk earth $^{232}Th/^{238}U$ value of 3.8. Errors are arbitrarily assumed to be 50%.

[a] $\delta\ ^{234}U = ([^{234}U/^{238}U]_{activity} - 1) \cdot 1000$.

[b] $\delta\ ^{234}U_{initial}$ was calculated based on ^{230}Th age (T), i.e., $d^{234}U_{initial} = d^{234}U_{measured} \cdot e^{l234 \cdot T}$.

[c] BP stands for Before Present where Present is the year 1950 CE.

the U/Th method, with dates spanning from 1 ± 2 ka to 524 ± 32 ka. The uncertainties (2σ) of seven speleothems represent 1%–4% of the obtained age, while the error of three datings (samples ZAM-02, NER-02A and Mar-01) accounts for 11%–17% of the obtained age. These uncertainties are considered acceptable for the purposes of the study. Only the most recent two samples exhibit a significant error, with values of 35% and 142% of the age, respectively. These discrepancies only indicate that these speleothems are very recent. The 12 dates

10969837, 2024, 11, Downloaded from https://onlinelibrary.wiley.com/doi/10.1002/esp.5915 by CochraneItalia, Wiley Online Library on [18/10/2024]. See the Terms and Conditions (https://onlinelibrary.wiley.com/terms-and-conditions) on Wiley Online Library for rules of use; OA articles are governed by the applicable Creative Commons License

revealed that speleothem formation along the Granada coast predominantly occurred during interglacial marine isotope stages (MIS) 13, 11, 7, 5 and 1, with few exceptions during glacial MIS 8 and 6.

5 | DISCUSSION

5.1 | Long-term subsidence in Granada coast

The geomorphological evidence (Section 4.1) indicates that the karst caves explored along the Granada coast originated within the vadose zone, above sea level. Furthermore, paleontological findings (Section 4.2) suggest a maximum age of 3.5–2.4 Ma for the Granada coast, while the minimum age exceeds 650 ka based on the oldest speleothems (Section 4.3). Consequently, it is reasonable to infer that the emergence and karstification of the Granada coast occurred within a time period between 3.5/2.4 Ma and 650 ka ago. Notably, the Calahonda karst contains vadose flowstone older than 650 ka and preserved within the present tidal zone. As this speleothem cannot have formed here (Ballesteros et al., 2017), these speleothems should precipitate during periods of lower relative sea levels.

The evidence of uplifting processes along the Granada coast (3.5–2.4 Ma to >650 ka) predates those observed in the neighbouring Málaga and Almería coasts (Figure 2B). The western Málaga coast was emerging during the Late Pleistocene (Lario et al., 1993) while the uplift affected the Campo de Dalías coastal plain in eastern Almería shore over the last 180 ka ago (Goy et al., 2003; Goy & Zazo, 1986; Hillaire-Marcel et al., 1986; Zazo et al., 1994, 2013; Zazo & Goy, 1989). Contrastingly, no evidence of coastal uplifting during the Late Pleistocene has been found in the Granada coast. The speleothems found in Granada coast, dating back more than 650 ka, have been reported at altitudes similar to the Upper Pleistocene sediments extensively documented in the Málaga and Almería coastlines (Figure 10). These chronological disparities observed among Málaga, Granada and Almería cannot be solely attributed to sea-level fluctuations. Given their proximity, these coastal regions are affected by

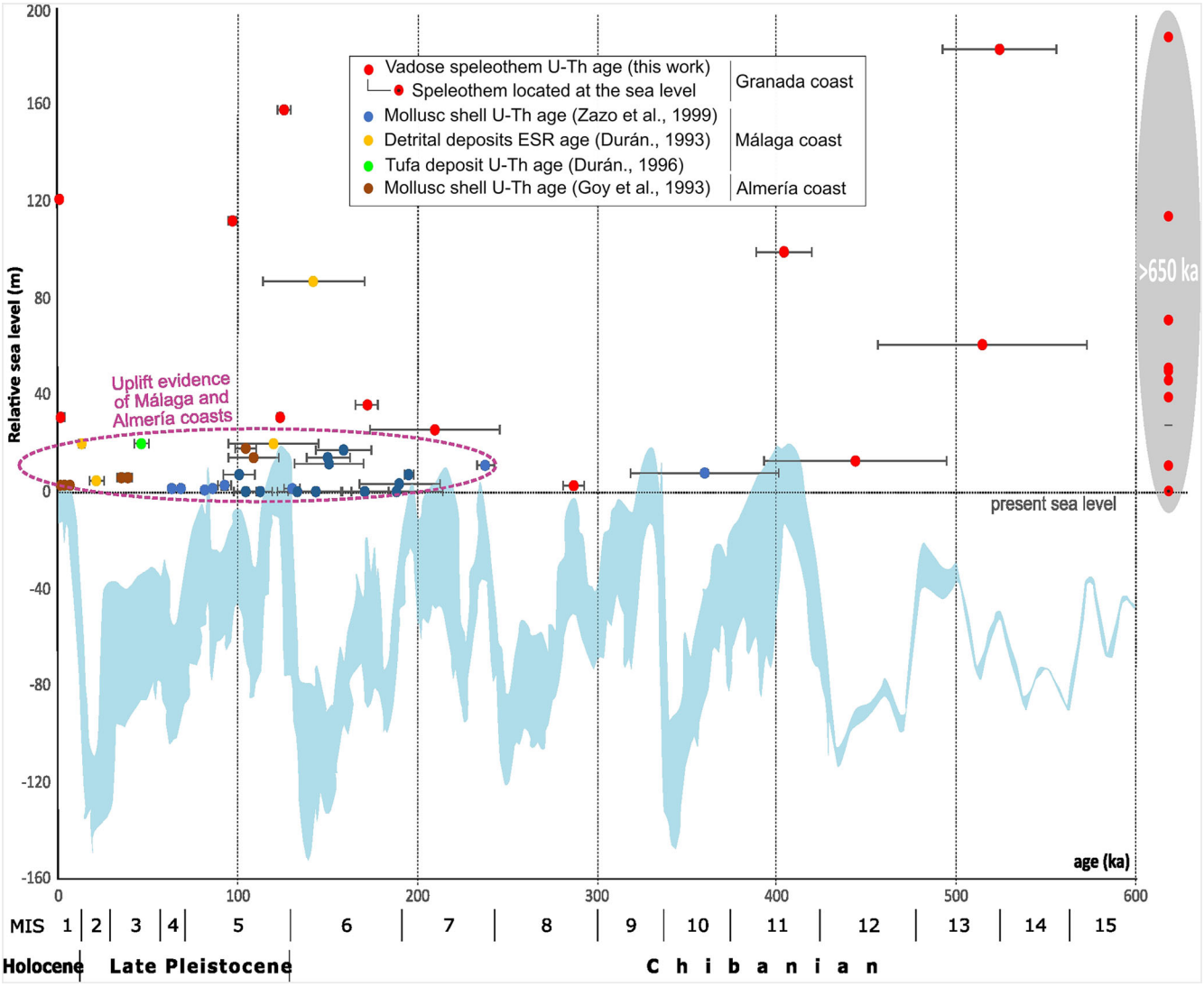

FIGURE 10 Vadose speleothems of the Granada coast (dated within this work), alongside uplift evidence from the Málaga and Almería shores, on the maximum relative sea-level oscillation envelope, as determined by relative sea-level (RSL) curves (Rabineau et al., 2006). Málaga and Almería coasts exhibit substantial uplift evidence since 200 ka, in contrast to the absence of reported uplift evidence along the Granada coast. [Color figure can be viewed at wileyonlinelibrary.com]

10969837, 2024, 11, Downloaded from https://onlinelibrary.wiley.com/doi/10.1002/esp.5915 by CochraneItalia, Wiley Online Library on [18/10/2024]. See the Terms and Conditions (https://onlinelibrary.wiley.com/terms-and-conditions) on Wiley Online Library for rules of use; OA articles are governed by the applicable Creative Commons License

similar eustatic influence. Hence, it is implied that tectonic processes impacted the Granada coast after its emergence and karstification. The tectonic movement should be a subsidence, which has led to the gradual descent of the coast, resulting in the repositioning of ancient speleothems to their current proximity to sea level.

The contemporary placement of vadose speleothems within the tidal zone of the Calahonda karst (Section 4.1) can be attributed to the subsidence phenomenon and sea-level oscillation, which combination is also plausible. These speleothems may have initially precipitated at higher elevations, descending gradually to their current location. Alternatively, they could have formed during a sea-level lowstand and later sea level raised up to the position of the speleothem. This explanation is unlikely because speleothem deposition typically occurs during interglacial stages (Figure 10), often coinciding with high sea levels (Aranburu et al., 2015).

The coastal subsidence hypothesis aligns with precise levelling data obtained by Giménez et al. (2000), spanning from the Almería shore to the eastern Málaga coast, which indicates a present-day relative general descent of the Granada coast at a rate of 1–2 mm·a^{-1}. At a local scale, this subsidence is concurrent with the Holocene marine transgression observed in the infralittoral and coastal deposits of Carchuna-Calahonda (e.g., Fernández-Salas et al., 2009), the progradation of the Guadalfeo delta (Jabaloy-Sánchez et al., 2014; Lobo et al., 2006) and the presence of buried shore platforms in Carchuna-Calahonda (Martínez-Martos et al., 2016). Although these abrasion platforms are currently situated 26–110 m below sea level, they likely formed near the mean high tidal mark and the wave base (Howell, 2005). Martínez-Martos et al. (2016) suggested that these buried shore platforms may have formed due to sea-level oscillations over the last approximately 150 ka, based on a comparison between the eroded platform positions and the relative sea-level (RSL) curve. However, there is a lack of dating evidence to support this chronology. Coastal subsidence may have contributed to the descent of these platforms after their formation in the nearshore environment.

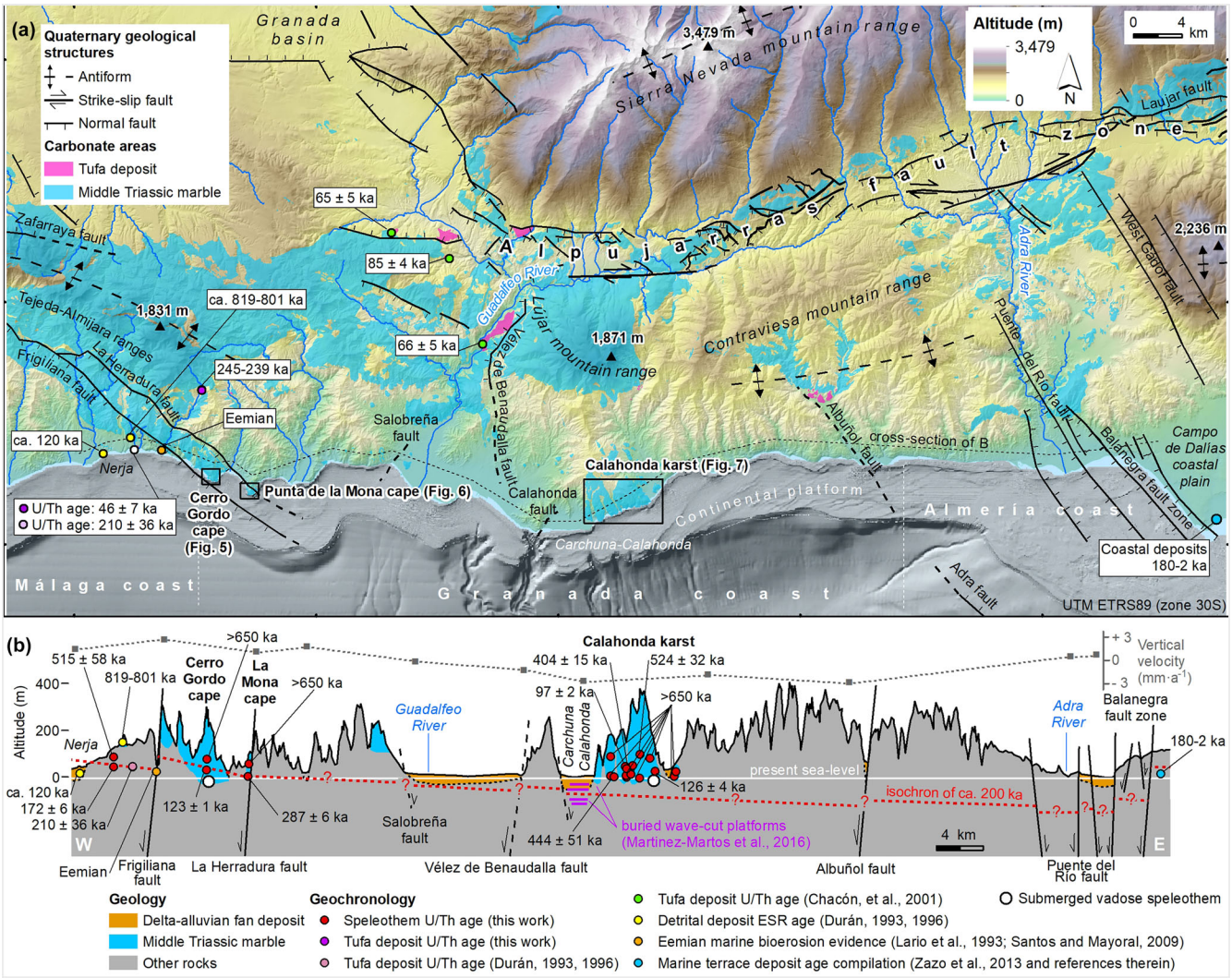

FIGURE 11 (a) Quaternary tectonic structures related to the subsidence of the Granada coast (see Section 2 of the supporting information). Carbonates extension is after Marín-Lechado et al. (2009) and bathymetry model is from *visor Cartografiado Marino* (www.infomar.miteco.es/visor.html) of Ministry of Agriculture, fisheries and food of Spain. The location of Figure 11a is shown in Figure 2b. (b) Speleothem ages (obtained in this work) and other chronological data projected on the cross-section along Málaga, Granada and Almería coast. Only the oldest date of Nerja cave (Durán, 1996) is depicted. Marble areas are represented schematically on the cross-section. The older speleothem isochrone of 200 ka (which means a past sea-level position) is approximately depicted to illustrate the subsiding processes and the potential effect of the Quaternary faults. Current vertical velocity recorded by Giménez et al. (2000) using topographic levelling are indicated. Vertical scale is exaggerated 20 times. [Color figure can be viewed at wileyonlinelibrary.com]

10969837, 2024, 11, Downloaded from https://onlinelibrary.wiley.com/doi/10.1002/esp.5915 by CochraneItalia, Wiley Online Library on [18/10/2024]. See the Terms and Conditions (https://onlinelibrary.wiley.com/terms-and-conditions) on Wiley Online Library for rules of use; OA articles are governed by the applicable Creative Commons License

5.2 | Unveiling the influence of active tectonics on coastal subsidence

Quaternary tectonic uplift has been observed in the limits among Málaga, Granada and Almería coasts (Figure 11a). The eastern boundary of the subsiding Granada coast aligns with the Balanegra active fault zone (BFZ) and other normal faults that contributed probably to the gradual sinking of the coast and the simultaneous uplift of the Campo de Dalías coastal plain along the Almería shore (Galindo-Zaldívar et al., 2013; Marín-Lechado et al., 2005, 2010; Martínez-Díaz & Hernández-Enrile, 2004) since approximately 180 ka (Goy & Zazo, 1986).

Figure 11b presents a cross-section along the Granada coastline, illustrating the speleothem dates obtained in this study along with other deposits dated in previous research. Additionally, the cross-section highlights the geological structures that explain the coastal subsidence. The former sea level is discerned through isochrones, defined by older speleothems along the coast. U/Th dating of coastal speleothems (Section 4.3) and previous geochronological data reveal an increase in age from Nerja (Málaga coast) to the Calahonda karst (Granada coast), indicating that older speleothem isochrones, such as the 200-ka isochrone (Figure 11b), are tilted toward the E. This inclination is likely associated with the BFZ and other normal faults along the Almería coast, which would displace the isochrone of 200 ka. Unfortunately, the exact vertical displacement caused by these faults cannot be precisely determined, but it is estimated to be less than 150 m during the Pleistocene, consistent with previous tectonic studies (Galindo-Zaldívar et al., 2003, 2013; Martínez-Díaz & Hernández-Enrile, 2004; Pedrera et al., 2012). At the boundary between the Málaga and Granada coasts, the 200-ka isochrone was likely influenced by the SW-dipping Frigiliana and La Herradura faults (Figure 11b), which exhibit extensional and oblique strike-slip movements (Ruano, 2004; Ruano et al., 2004). Both faults caused the elevation of Cerro Gordo and Punta de la Mona capes at the coastline.

5.3 | Coast evolution based on vadose karst deposits

The positioning in both space and time of the vadose speleothems, coupled with the unearthing of paleontological findings, and the discernment of active geological structures, collectively enable a comprehensive reconstruction of the tectonic history of the Granada coast, as illustrated in Figure 12. Faults become evident in the later stages of tectonic evolution, as indicated by sedimentary records (see Section 2 of the supporting information). However, faults may have been active even before their visible manifestation.

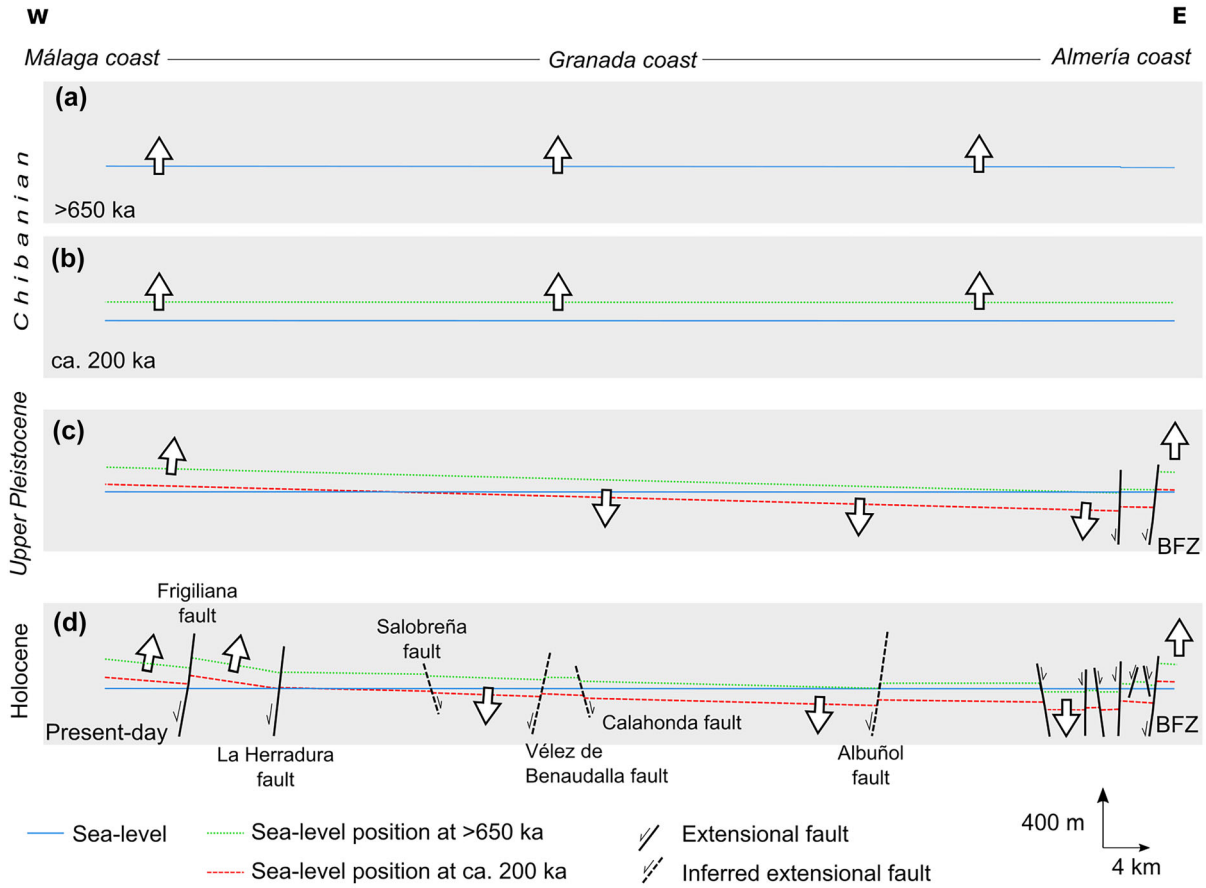

FIGURE 12 Tectonic contribution to the Quaternary evolution of Granada coast: (a) uplifting of Málaga, Granada and Almería coasts before 650 ka. (b) Coastal uplifting at ca. 200 ka. (c) Uplifting of Málaga and Almería coasts and subsiding of Granada shore after ca. 200 ka due to mainly Balanegra fault zone (BFZ). (d) Uplifting of the Málaga and Almería coasts and subsiding of Granada at present according to Figure 11b. The evolution of the coast is additionally influenced by minor faults, which are represented only in sections E and D for clarity. These structures may have been active in earlier stages. Fault vertical slips are tentative and are based on previous works detailed in Section 2 of the supporting information. Sea-level oscillations are not shown. Vertical scale is exaggerated 20 times. [Color figure can be viewed at wileyonlinelibrary.com]

10969837, 2024, 11, Downloaded from https://onlinelibrary.wiley.com/doi/10.1002/esp.5915 by CochraneItalia, Wiley Online Library on [18/10/2024]. See the Terms and Conditions (https://onlinelibrary.wiley.com/terms-and-conditions) on Wiley Online Library for rules of use; OA articles are governed by the applicable Creative Commons License

Following the coastal emergence prior to 650 ka (Figure 12a) and subsequent uplift until around 200 ka (Figure 12b), the Granada coast underwent descent and eastward inclination of ~0.15° due to the extensional activity of the BFZ. This resulted in an asymmetric subsidence pattern (Figure 12c,d). The BFZ has been active during the Late Pleistocene, supported by sedimentary and tectonic evidence in the Campo de Dalías coastal plain (Goy & Zazo, 1986; Hillaire-Marcel et al., 1986; Marín-Lechado et al., 2010; Pedrera et al., 2012; Zazo et al., 2003). Additionally, other extensional faults have led to local vertical displacements along the Granada coast, affecting Upper Pleistocene–Holocene coastal deposits (Bárcenas et al., 2011; Lario et al., 1995; Ortega-Sánchez et al., 2014). The isochrone of 200 ka may be impacted by these faults; however, the displacements are tentatively depicted in order to construct a cohesive evolutionary model. The Frigiliana faults, for instance, caused the uplift of the Cerro Gordo cape (Figure 11b) at a maximum rate of 0.28 $m \cdot a^{-1}$, as inferred from the altitude (35 m) and age (123 ± 1 ka) of speleothem GOR-12 found in Las Palomas marine cave (Sections 4.1 and 4.3). This uplift rate is comparable with the velocities of uplift reported in the western Málaga coast during the Quaternary (Figure 3; Durán, 1996). Ultimately, the subsidence of the Granada coast is linked to the westward displacements of the central Betic Cordillera relative to the stable Iberian Peninsula, influenced by extensional and strike-slip structures (e.g., Booth-Rea et al., 2004; de Lis Mancilla et al., 2015; Galindo-Zaldívar et al., 2022).

5.4 | Application of karst records on coastal subsiding research

Utilizing karst records to examine coastal subsidence provides valuable insights into the processes that have impacted the Granada coast since its emergence and karstification, driven by Quaternary extensional faulting. Despite the limited availability of onshore sedimentary records with chronological data, karst studies have yielded significant findings. Traditionally, flank margin and phreatic-epiphreatic caves are the go-to sources for inferring ancient sea levels (see Mylroie & Mylroie, 2018). However, following Van Hengstum et al. (2015) and Lucia et al. (2020), we took a different approach in our study by investigating the positions and ages of vadose speleothems and detrital deposits of continental origin. These data allow for the identification of previously emerged areas at various points in time, providing estimates of the minimum extent of the vadose zone over time. We have illustrated tentative isochrones that represent ancient sea levels by taking into account the age of the oldest speleothem at each elevation. This approach has also suggested the tilting of isochrones if speleothem ages are compared with previous chronologies along the coast, indicating the significant influence of the active Balanegra normal fault zone in the Campo de Dalías coastal plain.

While this method may not match the effectiveness of identifying and dating submerged marine terraces, tidal notches, flank margin caves and continental deposits, it has proven to be a valuable approach in cases where these features either do not exist or have not been recognized. Our approach hinges on comparing the timing of karst records from our study with the chronology of nearby coastal areas documented in previous research, underscoring the need of existing geochronological data. Furthermore, the applicability of karst investigations is constrained by the presence of accessible carbonate bed-rock along the coastline, which must contain suitable caves with speleothems and specific fossils. The commonly used U/Th dating technique does have its limitations, including the potential for detrital contamination as an additional source of Th; the requirement of a closed system to prevent post-depositional processes that might alter the initial concentration of U-series nuclides; and the constraint of being applicable only within a time range up to approximately 650 ka ago. It is worth noting that only 55% of the speleothems examined along the Granada coast yielded absolute dates through U/Th dating due to the limitations of this method. While the ICP-MS-based technique allows dating of speleothems younger than 650 ka (Cheng et al., 2013), other methods like U–Pb or U–U offer the potential to extend dating further back in time. However, their reliability depends on factors such as the concentrations of U and initial Pb, as well as the challenges associated with constraining the initial value of $\delta^{234}U$ (Wendt et al., 2021; Woodhead et al., 2006).

6 | CONCLUSIONS

Twenty-two new U/Th ages obtained from speleothems, along with the presence of *Iberus* fossils within karst infills, and existing geochronological data indicate that the Granada coast experienced subsidence following its emergence and karstification between 3.5/2.4 Ma and 650 ka. This subsidence is attributed to Quaternary extensional faults identified in previous tectonic studies. These faults resulted in the uplift of neighbouring areas while causing a lowering of the Granada coast, which lies in the hanging wall of faults developed to the N and E of the studied shore. Notably, the faults, such as the Balanegra fault zone (BFZ), also caused the paleo-coastlines to tilt towards the E.

This study demonstrates that karst records can serve as valuable indicators of subsidence processes in coastal regions. The use of vadose speleothems and terrestrial fossils enables the identification of the karst area that emerged over time. This involves establishing provisional isochrones based on the geochronological data gathered. These isochrones represent the lower boundary of the vadose zone for different times, effectively marking the water table and sea level at those points in time. In conclusion, our work introduces a novel approach of karst studies to understand the geomorphological evolution of coastal areas, particularly in areas where evidence of sea levels and coastal deposits are scarce.

AUTHOR CONTRIBUTIONS

José Miguel Azañón conceived the research, which was conducted by Daniel Ballesteros and funded by projects managed by Patricia Ruano and Jorge Pedro Galve. Marcos Moreno-Sánchez, Cristina Reyes-Carmona and Paula Sofía Jerez-Longres provided field and laboratory assistance. David Alfonso-Jorde prepared speleothem samples to be dated by Carlos Pérez-Mejías under the supervision of Hai Cheng. Diego Moreno identified paleontological findings. José Miguel Azañón, Patricia Ruano, Jorge Pedro Galve, Guillermo Booth-Rea, Antonio González-Ramón and Vicente Pérez-Peña contributed significantly to the results interpretation and discussion. Daniel Ballesteros and Carlos Pérez-Mejías wrote the first draft refined by all the authors.

10969837, 2024, 11, Downloaded from https://onlinelibrary.wiley.com/doi/10.1002/esp.5915 by CochraneItalia, Wiley Online Library on [18/10/2024]. See the Terms and Conditions (https://onlinelibrary.wiley.com/terms-and-conditions) on Wiley Online Library for rules of use; OA articles are governed by the applicable Creative Commons License

ACKNOWLEDGEMENTS

We are grateful to Grupo de Actividades Espeleológicas de Motril for providing cave data and supporting fieldwork. The research was supported by the following funds: European Regional Development Fund (ERDF) through the project 'RISKCOAST' (SOE3/P4/E0868) of the Interreg SUDOE Programme; the 'Ramón y Cajal' Programme (RYC-2017-23335) of the Spanish Ministry of Science; the project 'MORPHOMED' (PID2019-107138RB-I00) funded by Ministerio de Ciencia e Innovación (State Research Agency/10.13039/501100011033); FEDER/Junta de Andalucía-Consejería de Transformación Económica, Industria, Conocimiento y Universidades/Projects (B-RNM-305-UGR18, A-RNM-508-UGR20 and P18-RT-3632); and Plan Andaluz de Investigación, Desarrollo e Innovación 2020 (Junta de Andalucía). Consejería de Sostenibilidad, Medio Ambiente y Economía Azul (Junta de Andalucía) authorized the research within the Special Area of Conservation: Natural Site of Maro-Cerro Gordo Cliffs (ES6170002) and Cliff and Seabed of Punta de la Mona cape (ES6140016), Tesorillo-Salobreña (ES6140013), and Calahonda-Castell de Ferro (ES6140014).

DATA AVAILABILITY STATEMENT

The images showing the study caves are available in the supporting information. Other data are included in the article.

ORCID

Daniel Ballesteros https://orcid.org/0000-0002-2703-7730
Davide Torre https://orcid.org/0000-0001-8880-975X
Jorge Pedro Galve https://orcid.org/0000-0001-5780-821X

REFERENCES

Álvarez-Lao, D.J., Kahlke, R.D., García, N. & Mol, D. (2009) The Padul mammoth finds - on the southernmost record of *Mammuthus primigenius* in Europe and its southern spread during the Late Pleistocene. *Palaeogeography Palaeoclimatology Palaeoecology*, 278(1-4), 57–70. Available from: https://doi.org/10.1016/j.palaeo.2009.04.011

Anastasio, D.J., Pazzaglia, F.J., Parés, J.M., Kodama, K.P., Berti, C., Fisher, J.A., et al. (2021) Application of anisotropy of magnetic susceptibility (AMS) fabrics to determine the kinematics of active tectonics: examples from the Betic Cordillera, Spain, and the Northern Apennines, Italy. *Solid Earth*, 12(5), 1125–1142. Available from: https://doi.org/10.5194/se-12-1125-2021

Andreo, B., Barberá, J.A., Mudarra, M., Marín, A.I., García-Orellana, J., Rodellas, V., et al. (2018) A multi-method approach for groundwater resource assessment in coastal carbonate (karst) aquifers: the case study of Sierra Almijara (southern Spain). *Hydrogeology Journal*, 26(1), 41–56. Available from: https://doi.org/10.1007/s10040-017-1652-7

Andreucci, S., Sechi, D., Buylaert, J.P., Sanna, L. & Pascucci, V. (2017) Post-IR IRSL290 dating of K-rich feldspar sand grains in a wind-dominated system on Sardinia. *Marine and Petroleum Geology*, 87, 91–98. Available from: https://doi.org/10.1016/j.marpetgeo.2017.03.025

Aranburu, A., Arriolabengoa, M., Iriarte, E., Giralt, S., Yusta, I., Martínez-Pillado, V., et al. (2015) Karst landscape evolution in the littoral area of the Bay of Biscay (north Iberian Peninsula). *Quaternary International*, 364, 217–230. Available from: https://doi.org/10.1016/j.quaint.2014.09.025

Authemayou, C., Brocard, G., Delcaillau, B., Molliex, S., Pedoja, K., Husson, L., et al. (2018) Unraveling the roles of asymmetric uplift, normal faulting and groundwater flow to drainage rearrangement in an emerging karstic landscape. *Earth Surface Processes and Landforms*, 43(9), 1885–1898. Available from: https://doi.org/10.1002/esp.4363

Azañón, J.M. & Crespo-Blanc, A. (2000) Exhumation during a continental collision inferred from the tectonometamorphic evolution of the Alpujarride Complex in the central Betics (Alboran Domain, SE Spain). *Tectonics*, 19(3), 549–565. Available from: https://doi.org/10.1029/2000TC900005

Ballesteros, D., Jiménez-Sánchez, M., Giralt, S., García-Sansegundo, J. & Meléndez-Asensio, M. (2015) A multi-method approach for speleogenetic research on alpine karst caves. Torca La Texa shaft, Picos de Europa (Spain). *Geomorphology*, 247, 35–54. Available from: https://doi.org/10.1016/j.geomorph.2015.02.026

Ballesteros, D., Rodríguez-Rodríguez, L., González-Lemos, S., Giralt, S., Álvarez-Lao, D.J., Adrados, L., et al. (2017) New evidence of sea-level lowstands and paleoenvironment during MIS 6 and 4 in the Cantabrian coastal karst: the Cobiheru cave (North Iberia). *Earth Surface Processes and Landforms*, 42(11), 1704–1716. Available from: https://doi.org/10.1002/esp.4115

Bárcenas, P., Lobo, F.J., Macías, J., Fernández-Salas, L.M. & Díaz del Río, V. (2011) Spatial variability of surficial sediments on the northern shelf of the Alboran Sea: the effects of hydrodynamic forcing and supply of sediment by rivers. *Journal of Iberian Geology*, 37, 194–214. Available from: https://doi.org/10.5209/rev

Bardají, T., Cabero, A., Lario, J., Zazo, C., Silva, P.G., Goy, J.L., et al. (2015) Coseismic vs. climatic factors in the record of relative sea level changes: an example from the Last Interglacials in SE Spain. *Quaternary Science Reviews*, 113, 60–77. Available from: https://doi.org/10.1016/j.quascirev.2014.10.005

Bardají, T., Roquero, E., Cabero, A., Zazo, C., Goy, J.L., Dabrio, C.J. & Machado, M.J. (2022) Abrupt environmental changes during the last glacial cycle in Western Mediterranean (Formentera Island, Balearic archipelago, Spain). *Quarternary International*, 638-639, 159–179. Available from: https://doi.org/10.1016/j.quaint.2022.01.002

Barra, A., Reyes-Carmona, C., Herrera, G., Galve, J.P., Solari, L., Mateos, R.M., et al. (2022) From satellite interferometry displacements to potential damage maps: a tool for risk reduction and urban planning. *Remote Sensing of Environment*, 282, 113294. Available from: https://doi.org/10.1016/j.rse.2022.113294

Bergillos, R.J. & Ortega-Sánchez, M. (2017) Assessing and mitigating the landscape effects of river damming on the Guadalfeo River delta, southern Spain. *Landscape and Urban Planning*, 165, 117–129. Available from: https://doi.org/10.1016/j.landurbplan.2017.05.002

Bini, M., Zanchetta, G., Drysdale, R.N., Giaccio, B., Stocchi, P., Vacchi, M., et al. (2020) An end to the Last Interglacial highstand before 120 ka: Relative sea-level evidence from Infreschi Cave (Southern Italy). *Quaternary Science Reviews*, 250, 106658. Available from: https://doi.org/10.1016/j.quascirev.2020.106658

Blanco-Coronas, A.M., Calvache, M.L., López-Chicano, M., Martín-Montañés, C., Jiménez-Sánchez, J. & Duque, C. (2022) Salinity and temperature variations near the freshwater-saltwater interface in coastal aquifers induced by ocean tides and changes in recharge. *Water*, 14(18), 2807. Available from: https://doi.org/10.3390/w14182807

Blanco-Coronas, A.M., Duque, C., Calvache, M.L. & López-Chicano, M. (2021) Temperature distribution in coastal aquifers: insights from groundwater modelling and field data. *Journal of Hydrology*, 603, 126912. Available from: https://doi.org/10.1016/j.jhydrol.2021.126912

Booth-Rea, G., Azañón, J.M., Azor, A. & García-Dueñas, V. (2004) Influence of strike-slip fault segmentation on drainage evolution and topography. A case study: the Palomares Fault Zone (southeastern Betics, Spain). *Journal of Structural Geology*, 26(9), 1615–1632. Available from: https://doi.org/10.1016/j.jsg.2004.01.007

Calvache, M.L. & Pulido-Bosch, A. (1993) *The influence on the salt-water intrusion process of a karstified massif in a detrital system*. In: Custodio, E. & Galofré, A. (Eds.) Study and modelling of saltwater intrusion into aquifers. CIMNE, pp. 475–488.

Calvache, M.L. & Pulido-Bosch, A. (1997) Effects of geology and human activity on the dynamics of salt-water intrusion in three coastal aquifers in Southern Spain. *Environmental Geology*, 30(3–4), 215–223. Available from: https://doi.org/10.1007/s002540050149

10969837, 2024, 11, Downloaded from https://onlinelibrary.wiley.com/doi/10.1002/esp.5915 by CochraneItalia, Wiley Online Library on [18/10/2024]. See the Terms and Conditions (https://onlinelibrary.wiley.com/terms-and-conditions) on Wiley Online Library for rules of use; OA articles are governed by the applicable Creative Commons License

Calvache, M.L., Sánchez-Úbeda, J.P., Purtschert, R., López-Chicano, M., Martín-Montañés, C., Sültenfuβ, J., et al. (2020) Characterization of the functioning of the Motril–Salobreña coastal aquifer (SE Spain) through the use of environmental tracers. *Environment and Earth Science*, 79(6). Available from: https://doi.org/10.1007/s12665-020-8852-5

Camuera, J., Jiménez-Moreno, G., Ramos-Román, M.J., García-Alix, A., Toney, J.L., Anderson, R.S., et al. (2018) Orbital-scale environmental and climatic changes recorded in a new ~200,000-year-long multiproxy sedimentary record from Padul, southern Iberian Peninsula. *Quaternary Science Reviews*, 198, 91–114. Available from: https://doi.org/10.1016/j.quascirev.2018.08.014

Cerrillo-Escoriza, J., Lobo, J.L., Puga-Bernabéu, A., Rueda, J.L., Bárcenas, P., Sánchez-Guillamón, O., et al. (2023) Origin and driving mechanisms of marine litter in the shelf- incised Motril, Carchuna, and Calahonda canyons (northern Alboran Sea). *Frontiers in Marine Science*, *10*. Available from: https://doi.org/10.3389/fmars.2023.1098927

Cerrone, C., Vacchi, M., Fontana, A. & Rovere, A. (2021) Last Interglacial sea-level proxies in the western Mediterranean. *Earth System Science Data*, 13(9), 4485–4527. Available from: https://doi.org/10.5194/essd-13-4485-2021

Chacón, J., El Hamdouni, R., Irigaray, C., Delgado, A., Reyes, F., Fernández, T., et al. (2001) Valores de encajamiento de la red fuvial deducidos a partir del estudio de travertinos del valle del Lecrín y curso bajo del Guadalfeo (SE de Sierra Nevada, Granada). In: Sanz de Galdeano, C., Peláez, J.A. & Montilla, A.C. (Eds.) *La Cuenca de Granada: Estructura, Tectónica Activa, Sismicidad, Geomorfología y Dataciones Existentes*. Granada: Universidad de Granada, pp. 29–39.

Cheng, H., Edwards, R.L., Hoff, J., Gallup, C.D., Richards, D.A. & Asmerom, Y. (2000) The half-lives of U-234 and Th-230. *Chemical Geology*, 169(1-2), 17–33. Available from: https://doi.org/10.1016/S0009-2541(99)00157-6

Cheng, H., Edwards, R.L., Shen, C.C., Polyak, V.J., Asmerom, Y., Woodhead, J., et al. (2013) Improvements in ^{230}Th dating, ^{230}Th and ^{234}U half-life values, and U-Th isotopic measurements by multi-collector inductively coupled plasma mass spectrometry. *Earth and Planetary Science Letters*, 371–372, 82–91. Available from: https://doi.org/10.1016/j.epsl.2013.04.006

Corrado, G., Donadio, C., Pennetta, M., Schiattarella, M. & Valente, A. (2022) Pliocene to Quaternary morphotectonic evolution of the Gaeta Bay, Tyrrhenian coastal belt, central Italy: a review. *Quaternary International*, 638–639, 111–121. Available from: https://doi.org/10.1016/j.quaint.2022.05.010

Cunha, S., Silva, A., Flores Herráez, C., Pires, V., Chazarra, A., Mestre Barceló, A., et al. (2011) *Atlas Climático Ibérico-Iberian Climate Atlas*. Agencia Estatal de Meteorología, Instituto de Meteorologia de Portugal, Madrid, 79 p.

De Waele, J., D'Angeli, I.M., Bontognali, T.R.R., Tuccimei, P., Scholz, D., Jochum, K.P., et al. (2018) Speleothems in a north Cuban cave register sea-level changes and Pleistocene uplift rates. *Earth Surface Processes and Landforms*, 43, 2312–2326.

De Waele, J., D'Angeli, I.M., Tisato, N., Tuccimei, P., Soligo, M., Ginés, J., et al. (2017) Coastal uplift rate at Matanzas (Cuba) inferred from MIS5e phreatic overgrowths on speleothems. *Terra Nova*, 29(2), 98–105. Available from: https://doi.org/10.1111/ter.12253

Dumitru, O.A., Polyak, V.J., Asmerom, Y. & Onac, B.P. (2021) Last interglacial sea-level history from speleothems: a global standardized database. *Earth System Science Data*, 13(5), 2077–2094. Available from: https://doi.org/10.5194/essd-13-2077-2021

Durán, J.J. (1996) *Los sistemas kársticos de la provincia de Málaga y su evolución: contribución al conocimiento paleoclimático del Cuaternario en el Méditerráneo occidental. PhD Thesis*. Universidad Complutense de Madrid, Spain, 409 p.

Elejalde, M.A., Madeira, M.J., Arrébola, J.R., Muñoz, B. & Gómez-Moliner, B.J. (2008) Molecular phylogeny, taxonomy and evolution of the land snail genus Iberus (Pulmonata: Helicidae). *Journal of Zoological Systematics and Evolutionary Research*, 46(3), 193–202. Available from: https://doi.org/10.1111/j.1439-0469.2008.00468.x

Elejalde, M.A., Muñoz, B., Arrébola, J.R. & Gómez-Moliner, B.J. (2005) Phylogenetic relationships of *Iberus gualtieranus* and *I. alonensis* (Gastropoda: Helicidae) based on partial mitochondrial 16S rRNA and COI gene sequences. *Journal of Molluscan Studies*, 71(4), 349–355. Available from: https://doi.org/10.1093/mollus/eyi046

Faulkner, T. (2018) The ages of the Scandinavian caves. *Nor. Grottebl.*, 70, 15–33.

Fedje, D., Mackie, Q., McLaren, D., Wigen, B. & Southon, J. (2021) Karst caves in Haida Gwaii: archaeology and paleontology at the Pleistocene-Holocene transition. *Quaternary Science Reviews*, 272, 107221. Available from: https://doi.org/10.1016/j.quascirev.2021.107221

Fernández-Salas, L.M., Dabrio, C.J., Goy, J.L., Díaz del Río, V., Zazo, C., Lobo, F.J., et al. (2009) Land-sea correlation between Late Holocene coastal and infralittoral deposits in the SE Iberian Peninsula (Western Mediterranean). *Geomorphology*, 104(1-2), 4–11. Available from: https://doi.org/10.1016/j.geomorph.2008.05.013

Fernández-Salas, L.M., Lobo, F.J., Sanz, J.L., Díaz-del-Río, V., García, M.C. & Moreno, I. (2007) Morphometric analysis and genetic implications of pro-deltaic sea-floor undulations in the northern Alboran Sea margin, western Mediterranean Basin. *Marine Geology*, 243(1-4), 31–56. Available from: https://doi.org/10.1016/j.margeo.2007.04.013

Galindo-Zaldívar, J., Borque, M.J., Pedrera, A., Marín-Lechado, C., Gil, A.J. & López-Garrido, A.C. (2013) Deformation behaviour of the low-rate active Balanegra Fault Zone from high-precision levelling (Betic Cordillera, SE Spain). *Journal of Geodynamics*, 71, 43–51. Available from: https://doi.org/10.1016/j.jog.2013.07.003

Galindo-Zaldívar, J., Gil, A.J., Borque, J., Ercilla, G., Gonz, L., Alberto, S., et al. (2022) The Campo de Dalias GNSS network unveils the interaction between roll-back and indentation tectonics in the Gibraltar arc. *Sensors*, 22(6), 2128. Available from: https://doi.org/10.3390/s22062128

Galindo-Zaldívar, J., Gil, A.J., Borque, M.J., González-Lodeiro, F., Jabaloy, A., Marín-Lechado, C., et al. (2003) Active faulting in the internal zones of the central Betic Cordilleras (SE, Spain). *Journal of Geodynamics*, 36(1-2), 239–250. Available from: https://doi.org/10.1016/S0264-3707(03)00049-8

Galve, J.P., Pérez-Peña, J.V., Azañón, J.M., Closson, D., Caló, F., Reyes-Carmona, C., et al. (2017) Evaluation of the SBAS InSAR service of the European space agency's Geohazard Exploitation Platform (GEP). *Remote Sensing*, 9(12), 1291. Available from: https://doi.org/10.3390/rs9121291

Galve, J.P., Pérez-Peña, J.V., Azañón, J.M., Insua Pereira, D.M., Cunha, P.P., Pereira, P., et al. (2020) Active Landscapes of Iberia. In: Quesada, C. & Oliveira, J. (Eds.) *The geology of Iberia: a geodynamic approach*. Cham: Springer International Publishing, pp. 77–124. Available from: https://doi.org/10.1007/978-3-030-10931-8_5

Giménez, J., Suriñach, E. & Goula, X. (2000) Quantification of vertical movements in the eastern Betics (Spain) by comparing levelling data. *Tectonophysics*, 317(3-4), 237–258. Available from: https://doi.org/10.1016/S0040-1951(99)00318-2

Gómez de la Peña, L., Ranero, C.R., Gràcia, E. & Booth-Rea, G. (2021) The evolution of the westernmost Mediterranean basins. *Earth Science Reviews*, 214, 103445. Available from: https://doi.org/10.1016/j.earscirev.2020.103445

González-Ramón, A., López-Chicano, M., Gázquez, F., Durán-Valsero, J.J., Pedrera, A., Ruiz-Constán, A., et al. (2017) Isotopic and hydrochemistry spatial variation of sulfate for groundwater characterization in karstic aquifers. *Hydrological Processes*, 31(18), 3242–3254. Available from: https://doi.org/10.1002/hyp.11255

Goy, J.L. & Zazo, C. (1986) Synthesis of the Quaternary in the Almeria littoral neotectonic activity and its morphologic features, western Betics, Spain. *Tectonophysics*, 130(1-4), 259–270. Available from: https://doi.org/10.1016/0040-1951(86)90116-2

Goy, J.L. & Zazo, C. (1989) The role of neotectonics in the morphologic distribution of the Quaternary marine and continental deposits of the Elche Basin, southeast Spain. *Tectonophysics*, 163(3-4), 219–225. Available from: https://doi.org/10.1016/0040-1951(89)90259-X

10969837, 2024, 11, Downloaded from https://onlinelibrary.wiley.com/doi/10.1002/esp.5915 by CochraneItalia, Wiley Online Library on [18/10/2024]. See the Terms and Conditions (https://onlinelibrary.wiley.com/terms-and-conditions) on Wiley Online Library for rules of use; OA articles are governed by the applicable Creative Commons License

Goy, J.L., Zazo, C., Bardaji, T., Somoza, L., Causse, C. & Hillaire-Marcel, C. (1993) Eléments d'une chronostratigraphie du Tyrrhénien des régions d'Alicante-Murcie. *Sud-Est de l'Espagne, Geodinamica Acta*, 6(2), 103–119. Available from: https://doi.org/10.1080/09853111.1993.11105241

Goy, J.L., Zazo, C. & Dabrio, C.J. (2003) A beach-ridge progradation complex reflecting periodical sea-level and climate variability during the Holocene (Gulf of Almería, Western Mediterranean). *Geomorphology*, 050(1-3), 251–268. Available from: https://doi.org/10.1016/S0169-555X(02)00217-9

Guerra-Merchán, A., Serrano, F. & Ramallo, D. (2004) Geomorphic and sedimentary Plio-Pleistocene evolution of the Nerja area (northern Alboran basin, Spain). *Geomorphology*, 60(1-2), 89–105. Available from: https://doi.org/10.1016/j.geomorph.2003.07.010

Hillaire-Marcel, C., Carro, O., Causse, C., Goy, J.L. & Zazo, C. (1986) Th/U dating of Strombus bubonius- bearing in southeastern Spain marine terraces. *Geology*, 14(7), 613–616. Available from: https://doi.org/10.1130/0091-7613(1986)14<613:TDOSBM>2.0.CO;2

Howell, J. (2005) Sedimentary environments: shoreline and shoreface deposits. In: Selley, R.C., Cocks, L.R.M. & Plimer, I.R. (Eds.) *Encyclopedia of Geology*. Elsevier, Oxford, pp. 570–579. Available from: https://doi.org/10.1016/B0-12-369396-9/00494-9

Jabaloy-Sánchez, A., Lobo, F.J., Azor, A., Bárcenas, P., Fernández-Salas, L.M., del Río, V.D., et al. (2010) Human-driven coastline changes in the Adra River deltaic system, southeast Spain. *Geomorphology*, 119(1-2), 9–22. Available from: https://doi.org/10.1016/j.geomorph.2010.02.004

Jabaloy-Sánchez, A., Lobo, F.J., Azor, A., Martín-Rosales, W., Pérez-Peña, J.V., Bárcenas, P., et al. (2014) Six thousand years of coastline evolution in the Guadalfeo deltaic system (southern Iberian Peninsula). *Geomorphology*, 206, 374–391. Available from: https://doi.org/10.1016/j.geomorph.2013.08.037

Jaffey, A.H., Flynn, K.F., Glendenin, L.E., Bentley, W.C. & Essling, A.M. (1971) Precision measurement of half-lives and specific activities of ^{235}U and ^{238}U. *Physical Review C*, 4(5), 1889–1906. Available from: https://doi.org/10.1103/PhysRevC.4.1889

Jordá Pardo, J.F., Maestro González, A., Aura Tortosa, J.E., Álvarez Fernández, E., Avezuela Aristu, B., Badal García, E., et al. (2011) Evolución paleogeográfica, paleoclimática y paleoambiental de la costa meridional de la Península Ibérica durante el Pleistoceno superior. El caso de la Cueva de Nerja (Málaga, Andalucía, España). *Boletín la Real Soc. Española Hist. Nat. Sección Geológica*, 105, 137–147.

Kahlert, T., O'Donnell, S., Stimpson, C., Mai Hương, N.T., Hill, E., Utting, B., et al. (2021) Mid-Holocene coastline reconstruction from geomorphological sea level indicators in the Tràng An World Heritage Site, northern Vietnam. *Quaternary Science Reviews*, 263, 107001. Available from: https://doi.org/10.1016/j.quascirev.2021.107001

Kampolis, I., Triantafyllidis, S., Skliros, V. & Kamperis, E. (2022) Quaternary evolutionary stages of Selinitsa Cave (SW Peloponnese, Greece) reveal sea-level changes based on 3D scanning, geomorphological, biological, and sedimentological indicators. *Quaternary*, 5(2), 24. Available from: https://doi.org/10.3390/quat5020024

Kanwal, S., Ding, X., Wu, S. & Sajjad, M. (2022) Vertical ground displacements and its impact on erosion along the Karachi Coastline, Pakistan. *Remote Sensing*, 24, 2054.

Khan, N.S., Hibbert, F. & Rovere, A. (2019) Sea-level databases. *Pages Magazine*, 27 (1), 10–11.

Lario, J., Zazo, C., Dabrio, C.J., Somoza, L., Goy, J.L., Bardaji, T., et al. (1995) Record of recent Holocene sediment input on spit bars and deltas of South Spain. *Journal of Coastal Research, SI*, 17, 241–245.

Lario, J., Zazo, C., Somoza, L., Goy, J.L., Hoyos, M., Silva, P.G., et al. (1993) Los episodios marinos cuaternarios de la costa de Málaga (España). *Revista. Sociedad Geologica de España*, 6, 41–46.

Larrey, M., Mouthereau, F., Masini, E., Huyghe, D., Gaucher, E.C., Virgone, A., et al. (2020) Quaternary tectonic and climate changes at the origin of travertine and calcrete in the eastern betics (Almería region, SE Spain). *Journal of the Geological Society of London*, 177(5), 939–954. Available from: https://doi.org/10.1144/jgs2020-025

de Lis Mancilla, F., Stich, D., Morales, J., Martín, R., Diaz, J., Pazos, A., et al. (2015) Crustal thickness and images of the lithospheric discontinuities in the Gibraltar arc and surrounding areas. *Geophysical Journal International*, 203, 1804–1820. Available from: https://doi.org/10.1093/gji/ggv390

Lobo, F.J., Fernández-Salas, L.M., Moreno, I., Sanz, J.L. & Maldonado, A. (2006) The sea-floor morphology of a Mediterranean shelf fed by small rivers, northern Alboran Sea margin. *Continental Shelf Research*, 26(20), 2607–2628. Available from: https://doi.org/10.1016/j.csr.2006.08.006

López-Chicano, M., Calvache, M.L., Martín-Rosales, W. & Gisbert, J. (2002) Conditioning factors in flooding of karstic poljes - the case of the Zafarraya Polje (South Spain). *Catena*, 49(4), 331–352. Available from: https://doi.org/10.1016/S0341-8162(02)00053-X

López-Sánchez, C., Buforn, E., Cesca, S., Lozano, L., Sanz de Galdeano, C., Mattesini, M., et al. (2022) Intermediate-depth earthquakes in southern Spain and Alboran Sea. *Tectonophysics*, 825, 229238. Available from: https://doi.org/10.1016/j.tecto.2022.229238

Lucia, G., Polyak, V.J., Ginés, J., Fornós, J.J., Ginés, A., Asmerom, Y., et al. (2020) Chronology of Middle Pleistocene coastal karst evolution and relative sea-level changes in Mallorca. *Journal of Coastal Research*, 37(2), 408–420. Available from: https://doi.org/10.2112/JCOASTRES-D-20-00082.1

Madarieta-Txurruka, A., González-Castillo, L., Peláez, J.A., Catalán, M., Henares, J., Gil, A.J., et al. (2022) The role of faults as barriers in confined seismic sequences: 2021 seismicity in the Granada Basin (Betic cordillera). *Tectonics*, 41(9), e2022TC007481. Available from: https://doi.org/10.1029/2022TC007481

Marín-Lechado, C., Galindo-Zaldívar, J., Gil, A.J., Borque, M.J., de Lacy, M.C., Pedrera, A., et al. (2010) Levelling profiles and a GPS network to monitor the active folding and faulting deformation in the Campo de Dalias (Betic Cordillera, Southeastern Spain). *Sensors*, 10(4), 3504–3518. Available from: https://doi.org/10.3390/s100403504

Marín-Lechado, C., Galindo-Zaldívar, J., Rodríguez-Fernández, L.R., Serrano, I. & Pedrera, A. (2005) Active faults, seismicity and stresses in an internal boundary of a tectonic arc (Campo de Dalías and Níjar, southeastern Betic Cordilleras, Spain). *Tectonophysics*, 396(1-2), 81–96. Available from: https://doi.org/10.1016/j.tecto.2004.11.001

Marín-Lechado, C., Roldán García, F.J., Pineda Velasco, A., Martínez Zubieta, P., Rodero Pérez, J. & Pinto, D. (2009) Mapa Geológico Digital continuo E. 1: 50.000, Zonas internas de las Cordilleras Béticas. (Zona-2100). In: Navas, J. (Ed.) *GEODE. Mapa Geológico Digital Continuo de España. [On-line]. Sistema de Información Geológica Continua: SIGECO*. Madrid: Instituto Geológico y Minero de España.

Martínez-Díaz, J.J. & Hernández-Enrile, J.L. (2004) Neotectonics and morphotectonics of the southern Almería region (Betic Cordillera-Spain) kinematic implications. *International Journal of Earth Sciences*, 93(2), 189–206. Available from: https://doi.org/10.1007/s00531-003-0379-y

Martínez-Martos, M., Galindo-Zaldívar, J., Lobo, F.J., Pedrera, A., Ruano, P., López-Chicano, M., et al. (2016) Buried marine-cut terraces and submerged marine-built terraces: the Carchuna-Calahonda coastal area (southeast Iberian Peninsula). *Geomorphology*, 264, 29–40. Available from: https://doi.org/10.1016/j.geomorph.2016.04.010

Martos-Rosillo, S., González-Ramón, A., Jiménez-Gavilán, P., Andreo, B., Durán, J.J. & Mancera, E. (2015) Review on groundwater recharge in carbonate aquifers from SW Mediterranean (Betic Cordillera, S Spain). *Environment and Earth Science*, 74(12), 7571–7581. Available from: https://doi.org/10.1007/s12665-015-4673-3

Mateos, R.M., Azañón, J.M., Roldán, F.J., Notti, D., Pérez-Peña, V., Galve, J.P., et al. (2017) The combined use of PSInSAR and UAV photogrammetry techniques for the analysis of the kinematics of a coastal landslide affecting an urban area (SE Spain). *Landslides*, 14(2), 743–754. Available from: https://doi.org/10.1007/s10346-016-0723-5

Mattei, G., Caporizzo, C., Corrado, G., Vacchi, M., Stocchi, P., Pappone, G., et al. (2022) On the influence of vertical ground movements on Late-Quaternary sea-level records. A comprehensive assessment along the mid- Tyrrhenian coast of Italy (Mediterranean Sea). *Quaternary*

10969837, 2024, 11, Downloaded from https://onlinelibrary.wiley.com/doi/10.1002/esp.5915 by CochraneItalia, Wiley Online Library on [18/10/2024]. See the Terms and Conditions (https://onlinelibrary.wiley.com/terms-and-conditions) on Wiley Online Library for rules of use; OA articles are governed by the applicable Creative Commons License

Science Reviews, 279, 107384. Available from: https://doi.org/10.1016/j.quascirev.2022.107384

Medina-Cascales, I., García-Tortosa, F.J., Martin-Rojas, I., Pérez-Peña, J.V. & Alfaro, P. (2021) Tectonic geomorphology of an active slow-moving, intrabasinal fault: the Galera Fault (Guadix-Baza Basin, central Betic Cordillera, southern Spain). *Geomorphology*, 393, 107941. Available from: https://doi.org/10.1016/j.geomorph.2021.107941

Montiel, D., Dimova, N., Andreo, B., Prieto, J., García-Orellana, J. & Rodellas, V. (2018) Assessing submarine groundwater discharge (SGD) and nitrate fluxes in highly heterogeneous coastal karst aquifers: challenges and solutions. *Journal of Hydrology*, 557, 222–242. Available from: https://doi.org/10.1016/j.jhydrol.2017.12.036

Moragues, L., Ruano, P., Azañón, J.M., Garrido, C.J., Hidas, K. & Booth-Rea, G. (2021) Two Cenozoic extensional phases in Mallorca and their bearing on the geodynamic evolution of the Western Mediterranean. *Tectonics*, 40(11), e2021TC006868. Available from: https://doi.org/10.1029/2021TC006868

Mylroie, J.E. & Mylroie, J.R. (2018) Role of karst denudation on the accurate assessment of glacio-eustasy and tectonic uplift on carbonate coasts. *Geological Society - Special Publications*, 466(1), 171–185. Available from: https://doi.org/10.1144/SP466.2

Mylroie, J., Mylroie, J., Humphreys, W., Brooks, D. & Middleton, G. (2017) Flank margin cave development and tectonic uplift, cape range, Australia. *Journal of Cave and Karst Studies*, 79(1), 35–47. Available from: https://doi.org/10.4311/2015ES0142

Neiber, M.T., Chueca, L.J., Caro, A., Teixeira, D., Schlegel, K.A., Gómez-Moliner, B.J., et al. (2021) Incorporating palaeogeography into ancestral area estimation can explain the disjunct distribution of land snails in Macaronesia and the Balearic Islands (Helicidae: Allognathini). *Molecular Phylogenetics and Evolution*, 162, 107196. Available from: https://doi.org/10.1016/j.ympev.2021.107196

Notti, D., Galve, J.P., Mateos, R.M., Monserrat, O., Lamas-Fernández, F., Fernández-Chacón, F., et al. (2015) Human-induced coastal landslide reactivation. Monitoring by PSInSAR techniques and urban damage survey (SE Spain). *Landslides*, 12(5), 1007–1014. Available from: https://doi.org/10.1007/s10346-015-0612-3

Ortega-Sánchez, M., Lobo, F.J., López-Ruiz, A., Losada, M.A. & Fernández-Salas, L.M. (2014) The influence of shelf-indenting canyons and infralittoral prograding wedges on coastal morphology: the Carchuna system in southern Spain. *Marine Geology*, 347, 107–122. Available from: https://doi.org/10.1016/j.margeo.2013.11.006

Pedrera, A., Marín-Lechado, C., Stich, D., Ruiz-Constán, A., Galindo-Zaldívar, J., Rey-Moral, C., et al. (2012) Nucleation, linkage and active propagation of a segmented Quaternary normal-dextral fault: the Loma del Viento fault (Campo de Dalías, Eastern Betic Cordillera, SE Spain). *Tectonophysics*, 522–523, 208–217. Available from: https://doi.org/10.1016/j.tecto.2011.12.001

Porras, D., Carrasco, J., Carrasco, P. & González, P.J. (2022) Imaging extensional fault systems using deep electrical resistivity tomography: a case study of the Baza fault, Betic cordillera, Spain. *Journal of Applied Geophysics*, 202, 104673. Available from: https://doi.org/10.1016/j.jappgeo.2022.104673

Rabineau, M., Berné, S., Olivet, J.L., Aslanian, D., Guillocheau, F. & Joseph, P. (2006) Paleo sea levels reconsidered from direct observation of paleoshoreline position during Glacial Maxima (for the last 500,000 yr). *Earth and Planetary Science Letters*, 252(1-2), 119–137. Available from: https://doi.org/10.1016/j.epsl.2006.09.033

Rovere, A., Ryan, D.D., Vacchi, M., Dutton, A., Simms, A.R. & Murray-Wallace, C.V. (2023) The world atlas of last interglacial shorelines (version 1.0). *Earth Systems*, 15, 1–23.

Ruano, P. (2004) *Estructuras tectónicas recientes en la transversal central de las Cordilleras Béticas*. Madrid: Instituto Geológico y Minero de España, p. 498.

Ruano, P., Galindo-Zaldívar, J. & Jabaloy, A. (2004) Recent tectonic structures in a transect of the central Betic cordillera. *Pure and Applied Geophysics*, 161(3), 541–563. Available from: https://doi.org/10.1007/s00024-003-2462-5

Salgado-Garrido, H.E., Valera-Fernández, D., Trejo-Pelayo, S., Solleiro-Rebolledo, E., Barragán, R., Yáñez-Mendoza, G., et al. (2022) The microfacies distribution pattern of Cozumel Island in southeastern Mexico: an atoll-like model led by Quaternary glacioeustatic sea-level changes. *Journal of South American Earth Sciences*, 118, 103933. Available from: https://doi.org/10.1016/j.jsames.2022.103933

Sanz de Galdeano, C. (2006) Formas de erosión marinas en el sector comprendido entre Maro y Castell de Ferro (Costa de Málaga y Granada). *Geogaceta*, 39, 139–142.

Serrano, M.A., Cobos, M., Magaña, P.J. & Díez-Minguito, M. (2020) Sensitivity of Iberian estuaries to changes in sea water temperature, salinity, river flow, mean sea level, and tidal amplitudes. *Estuarine, Coastal and Shelf Science*, 236, 106624. Available from: https://doi.org/10.1016/j.ecss.2020.106624

Simancas, J.F. (2018) A reappraisal of the alpine structure of the Alpujárride complex in the Betic Cordillera: interplay of shortening and extension in the westernmost Mediterranean. *Journal of Structural Geology*, 115, 231–242. Available from: https://doi.org/10.1016/j.jsg.2018.08.001

Smith, M.P. & Moseley, G.E. (2022) The karst and palaeokarst of North and North-East Greenland – physical records of cryptic geological intervals. *GEUS Bulletin*, 49, 1–23. Available from: https://doi.org/10.34194/geusb.v49.8298

Tendero-Salmerón, V., Galindo-Zaldívar, J., Peláez, J.A., Martínez-Martos, M., Henares, J., Marín-Lechado, C., et al. (2020) Seismicity in strike-slip foreland faults (Central Betic Cordillera front): evidence of indentation tectonics. *Tectonics*, 39(7), e2020TC006143. Available from: https://doi.org/10.1029/2020TC006143

Valera-Fernández, D., Solleiro-Rebolledo, E., López-Martínez, R., Sedov, S. & Cabadas-Baéz, H. (2022) Quaternary paleoenvironments based on pedogenic, sedimentary and karstic processes in the coastal geosystems of Cozumel Island, Mexcio. *Geoderma Regional*, 31, e00587. Available from: https://doi.org/10.1016/j.geodrs.2022.e00587

Van Hengstum, P.J., Richards, D.A., Onac, B.P. & Dorale, J.A. (2015) Handbook of Sea-level Research. In: Shennan, I., Long, A.J. & Horton, B.P. (Eds.) *Handbook of sea-level research*, pp. 83–103. Available from: https://doi.org/10.1002/9781118452547.ch6

Weij, R., Woodhead, J.D., Sniderman, J.M.K., Hellstrom, J.C., Reed, E., Bourne, S., et al. (2022) Cave opening and fossil accumulation in Naracoorte, Australia, through charcoal and pollen in dated speleothems. *Communications Earth & Environment*, 3, 1–8.

Wendt, K.A., Li, X. & Edwards, R.L. (2021) Uranium–thorium dating of speleothems. *Elements*, 17, 87–92.

Woodhead, J., Hellstrom, J., Maas, R., Drysdale, R., Zanchetta, G., Devine, P., et al. (2006) U-Pb geochronology of speleothems by MC-ICPMS. *Quaternary Geochronology*, 1(3), 208–221. Available from: https://doi.org/10.1016/j.quageo.2006.08.002

Woodhead, J., Sniderman, K., Hellstrom, J., Weij, R., MacGregor, C., Dickson, B., et al. (2022) Timescales of speleogenesis in an evolving syngenetic karst: the Tamala Limestone, Western Australia. *Geomorphology*, 399, 108079. Available from: https://doi.org/10.1016/j.geomorph.2021.108079

Zazo, C., Dabrio, C.J., Goy, J.L., Lario, J., Cabero, A., Silva, P.G., et al. (2008) The coastal archives of the last 15 ka in the Atlantic-Mediterranean Spanish linkage area: sea level and climate changes. *Quaternary International*, 181(1), 72–87. Available from: https://doi.org/10.1016/j.quaint.2007.05.021

Zazo, C. & Goy, J.L. (1989) Sea-level changes in the Iberian Peninsula during the last 200,000 years. In: Scott, D.B. (Ed.) *Late Quaternary Sea-Level Correlations and Applications*. Dordrecht: Kluwer Academic Publishers, pp. 27–39. Available from: https://doi.org/10.1007/978-94-009-0873-4_2

Zazo, C., Goy, J.L. & Aguirre, E. (1984) Did Strombus survive the Last Interglacial in the Western Mediterranean Sea? *Serie de Estudios Geológicos*, 3, 131–137.

Zazo, C., Goy, J.L., Dabrio, C.J., Bardají, T., Hillaire-Marcel, C., Ghaleb, B., et al. (2003) Pleistocene raised marine terraces of the Spanish Mediterranean and Atlantic coasts: records of coastal uplift, sea-level highstands and climate changes. *Marine Geology*, 194(1-2), 103–133. Available from: https://doi.org/10.1016/S0025-3227(02)00701-6

10969837, 2024, 11, Downloaded from https://onlinelibrary.wiley.com/doi/10.1002/esp.5915 by CochraneItalia, Wiley Online Library on [18/10/2024]. See the Terms and Conditions (https://onlinelibrary.wiley.com/terms-and-conditions) on Wiley Online Library for rules of use; OA articles are governed by the applicable Creative Commons License

Zazo, C., Goy, J.L., Dabrio, C.J., Lario, J., González-Delgado, J.A., Bardají, T., et al. (2013) Retracing the Quaternary history of sea-level changes in the Spanish Mediterranean-Atlantic coasts: geomorphological and sedimentological approach. *Geomorphology*, 196, 36–49. Available from: https://doi.org/10.1016/j.geomorph.2012.10.020

Zazo, C., Goy, J.L., Somoza, L., Dabrio, C.J., Belluomini, G., Improta, S., et al. (1994) Holocene sequence of sea-level fluctuations in relation to climatic trends in the Atlantic-Mediterranean linkage coast. *Journal of Coastal Research*, 10, 933–945.

Zazo, C., Silva, P.G., Goy, J.L., Hillaire-Marcel, C., Ghaleb, B., Lario, J., et al. (1999) Coastal uplift in continental collision plate boundaries: data from the Last Interglacial marine terraces of the Gibraltar Strait area (south Spain). *Tectonophysics*, 301(1-2), 95–109. Available from: https://doi.org/10.1016/S0040-1951(98)00217-0

SUPPORTING INFORMATION

Additional supporting information can be found online in the Supporting Information section at the end of this article.

How to cite this article: Ballesteros, D., Pérez-Mejías, C., Moreno, D., Moreno-Sánchez, M., Reyes-Carmona, C., Alfonso-Jorde, D. et al. (2024) Unveiling the potential of karst vadose deposits in constraining Quaternary tectonic subsidence. *Earth Surface Processes and Landforms*, 49(11), 3437–3455. Available from: https://doi.org/10.1002/esp.5915

10969837, 2024, 11, Downloaded from https://onlinelibrary.wiley.com/doi/10.1002/esp.5915 by CochraneItalia, Wiley Online Library on [18/10/2024]. See the Terms and Conditions (https://onlinelibrary.wiley.com/terms-and-conditions) on Wiley Online Library for rules of use; OA articles are governed by the applicable Creative Commons License